IEEE P802.15
Wireless Personal Area Networks

Project	IEEE P802.15 Working Group for Wireless Personal Area Networks (WPANs)	
Title	Channel Models for WBANs – NICT	
Date Submitted	[7 November, 2008]	
Source	[Takahiro Aoyagi, Jun-ichi Takada, Kenichi Takizawa, Hirokazu Sawada, Norihiko Katayama, Kamya Yekeh Yazdandoost, Takehiko Kobayashi, Huan-Bang Li, and Ryuji Kohno] NICT 3-4 Hikarino-oka Yokosuka 2390847 Japan	Voice : +81-46-847-5432 Fax : +31-46-847-5431 E-mail: [aoyagi@nict.go.jp]
Re:	[Body Area Network (BAN) Channel Model document]	
Abstract	[This is a contribution to make a channel for wearable and implantable WBAN. It provides how channel model should be developed for wireless body area network.	
Purpose	[The purpose of this document is to provide the work of the channel modeling subcommittee and recommendations on how the channel model for BAN can be used.	
Notice	This document has been prepared to assist the IEEE P802.15. It is offered as a basis for discussion and is not binding on the contributing individual(s) or organization(s). The material in this document is subject to change in form and content after further study. The contributor(s) reserve(s) the right to add, amend or withdraw material contained herein.	
Release	The contributor acknowledges and accepts that this contribution becomes the property of IEEE and may be made publicly available by P802.15.	

Date	Revision No.
09/29/2008	15-08-0416-03-0006
11/07/2008	15-08-0416-04-0006

Table of Contents

1. Introduction

This document presents channel models for the IEEE802.15.6. The scenario for the channel models are based on Channel model subcommittee report [1]. The models shown in this document include CM3 (body surface to body surface) and CM4 (body surface to external). Also, informative material useful to derive CM2 (implant to body surface) is included. In Table 1, frequency bands which are provided as channel models in this document are shown for each channel model. On the channel modeling for CM2, its frequency band is 400 MHz, which includes MICS band. For the CM3, we measure the frequency bands of 400, 600, and 900 MHz, 2.4GHz and UWB. CM4 is available in UWB band. From the following section, channel models corresponding to CM2, CM3 and CM4 are illustrated.

Table 1: List of scenarios and their descriptions

Channel Model	Description	Frequency band(s)
CM2	Implant to Body Surface	400 MHz
CM3	Body Surface to Body Surface (LOS)	400, 600, 900 MHz 2.4 GHz UWB
	Body Surface to Body Surface (NLOS)	
CM4	Body Surface to External (LOS)	UWB
	Body Surface to External (NLOS)	

2. Channel Model CM3 for 400, 600, and 900 MHz and UWB Band

In this section, channel models for the CM3 are presented. The CM3 channel model consists of path loss models and a power delay profile model. The path loss models are derived for all the frequency bands we measured. On the other hand, the power delay profile model is only for the UWB band.

2.1 Measurement setup

The measurements are done in a hospital room environment. Figure 1 shows positions where the antennas are placed on the human body. The positions marked by ‘o’ are chosen so as to agree with locations where the WBAN devices will be attached. The location marked by ‘●’ represents assumed position of the WBAN coordinator.

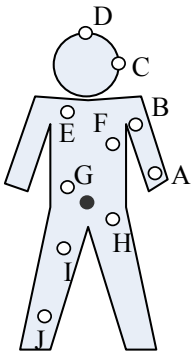

(a) Measurement positions on the human body

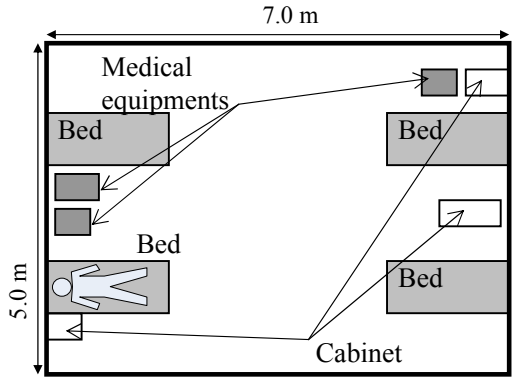

(b) Layout of the measurement room (a hospital room)

(c) Photograph at the measurement

Figure 1: Experiment setup: measurement locations on the human body (A: left wrist, B: left upper arm, C: left ear, D: head, E: shoulder, F: chest, G: right rib, H: left waist, I: Thigh, J: Ankle). Layout in the measurement cite, and photographs taken in the measurement.

Table 1: VNA setting, frequency bands and type of the used antennas.

(a) VNA setting

Parameter	Value
VNA	Agilent E8363B
The number of points	801 (400, 600,900, 2400 MHz) 3201 (UWB)
Sweep time	Auto
Calibration	Full-2-port (Tx power = 0 dBm)

(b) Measurement specifications

Frequency band	Frequency range	Antenna
400 MHz	420 - 450 MHz	 Chip antenna
600 MHz	608 - 614 MHz	(Its outlook is the same as that for 400 MHz) Chip antenna
900 MHz	950 - 956 MHz	(Its outlook is the same as that for 400 MHz) Chip antenna
2400 MHz	2400 - 2500 MHz	 Chip antenna
UWB	3000 – 11000 MHz	 Skycross™ antenna

Table 2: Distances between the two body-worn antennas in both measurement cites

(a) Anechoic chamber

Position index	Position	Distance *d* [mm]				
		400 MHz	600 MHz	900 MHz	2.4 GHz	UWB
A-1	Left hand	425	424	424	428	430
A-2	Left hand	400	402	400	422	402
B	Left upper arm	352	364	354	372	360
C	Left ear	582	608	588	578	582
D	Head	724	756	746	740	722
E	Shoulder	384	410	384	384	390
F	Chest	252	246	242	224	236
G	Right rib	171	154	146	148	155
H	Left waist	158	174	186	176	184
I	Thigh	396	388	404	404	402
J	Ankle	984	986	982	972	986

(b) Hospital room

Position index	Position	Distance *d* [mm]				
		400 MHz	600 MHz	900 MHz	2.4 GHz	UWB
A-1	Left hand	415	422	410	408	410
A-2	Left hand	392	408	388	386	390
B	Left upper arm	404	410	424	414	424
C	Left ear	575	576	578	562	570
D	Head	726	734	742	734	742
E	Shoulder	370	382	400	392	402
F	Chest	258	250	266	248	258
G	Right rib	170	154	174	170	176
H	Left waist	174	182	164	174	180
I	Thigh	394	404	388	402	400
J	Ankle	1002	1000	980	998	984

The measurements have been conducted in a hospital room, as shown in Figure 1, and an anechoic chamber. Although anechoic chambers are special environments, channel models based on the measured results in an anechoic chamber are provided to show the models where there are no reflections from surroundings.

The positions on body in the measurements are chosen so as to cover the most of applications shown in the 15.6 Application Matrices [2].

An S-parameter S21 which is essentially corresponds to the channel transfer function (CTF) are measured by a vector network analyzer (VNA). Table 1(a) listed a setting of the VNA, and Table 1(b) gives information on the measured frequency band and used antennas. As shown in Table 1, a chip antenna is used for each measurement in 400, 600 and 900 MHz, and 2.4-GHz band. For the measurement in the UWB band, Skycross antenna is used. The frequency bands are selected so as to include most frequency bands that are reported in the 15.6 Regulation Document [3].

Distances between the two body-worn antennas are summarized in Table 2. In these tables, you can find difference between distances at the same position. This is due to the difference of the antenna size for different frequency bands. Note that, at the position 'A', we measured CTFs in

two different ways; one is that the antenna is attached to the flank side ('A-1'), and the other one attaches the antenna to the front side ('A-2'). Through all the measurements, 15-mm separation between body surface and worn antenna is maintained.
The height and weight of the volunteer participating in this experiment are 173 cm and 64 kg, respectively; these values are typical of healthy Japanese males. S21 is measured 10 times at each position and each frequency band.
Measured path loss for each frequency bands and snapshot are shown in Fig. 2. In these results, antenna gain at both Tx and Rx are not removed, because antenna characteristics are highly effected by human body in BAN. The path gain at a frequency *f*, position *p*, and *j* th snapshot is obtained by

$$PL_j^p(f) = 10\log_{10}\left|H_j^p(f)\right|^2, \quad p \in \{\mathrm{A}-1, \mathrm{A}-2, \cdots, \mathrm{J}\} \ \ [\mathrm{dB}] \qquad (1)$$

where $H_j^p(f)$ denotes the measured S21 through the setup shown in Fig. 1. Shown results on the measured path loss confirm that the CTFs for the frequency bands except the UWB band are flat responses. This means that the bands except UWB band requires only path loss model. On the other hand, the UWB band requires not only a path loss model but also a power delay profile (PDP) model.

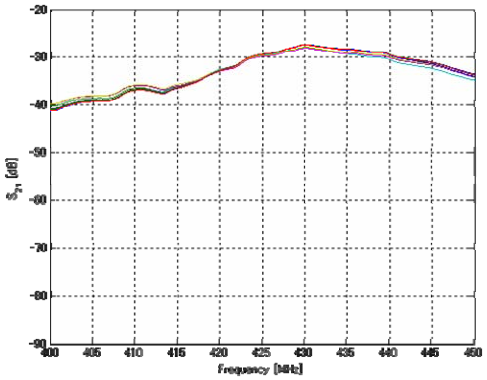

(a) 400MHz

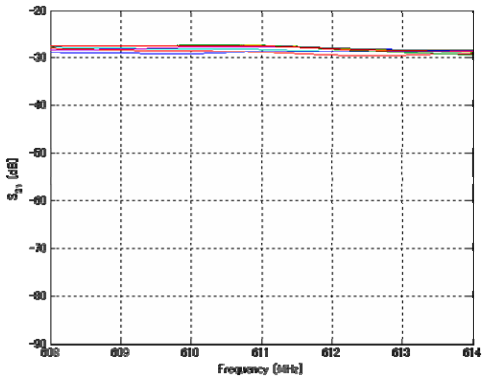

(b) 600MHz

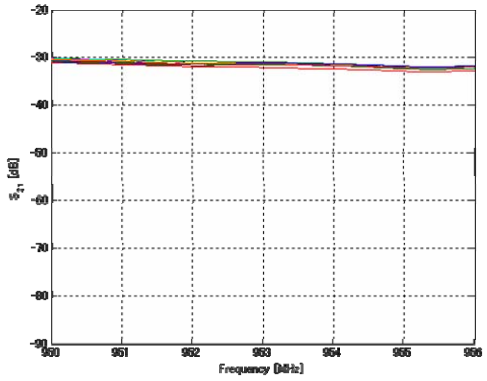

(c) 900MHz

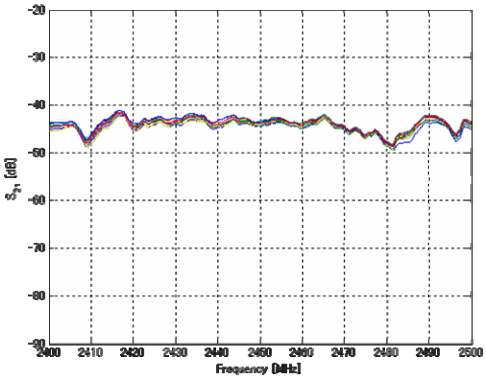

(d) 2.4GHz

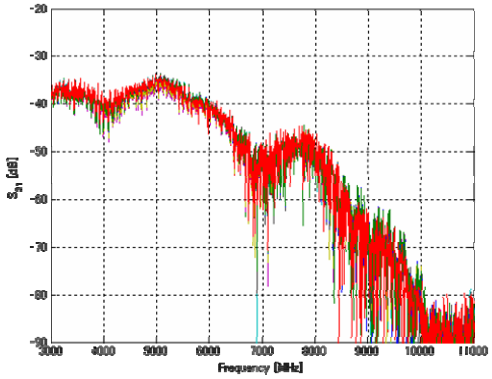

(e) UWB

Figure 2: Measured path gain in the frequency bands of 400, 600, and 900 MHz, 2.4 GHz, and UWB. The separation between body surface and body-worn antenna is 15 mm. These results are measured at position 'f' (Rx antenna is attached to the chest position). Other measured results are summarized in Appendix A. 1.

3.2 Path loss model

In this section, path loss models for the frequency bands are shown.
The path loss model is simply written as follows:

$$L_{\text{path}}(d) = a \cdot \log_{10} d + b + N \quad [\text{dB}] \qquad (2)$$

where $L_{\text{path}}(d)$ means the path loss in dB at a distance d mm. a and b denote parameters derived by a least square fitting to the measured average path loss over the frequency range, ${l_{\text{path}}}^{p}{}_{j}(d)$, which is given by

$${l_{\text{path}}}^{p}{}_{j}(d) = -10 \cdot \log_{10}\left\{\frac{1}{N_{\text{F}}}\sum_{m=1}^{N_F} {PL}^{p}{}_{j}\left(f(m)\right)\right\} \quad [\text{dB}] \qquad (3)$$

where f_m stands for a frequency which corresponds to the m th sample point at the measurement. In Eq. (2), N is a stochastic term which has a log-normal distribution with zero-mean and standard deviation of σ_N.
Figure 3 shows the measured each path loss ${l_{\text{path}}}^{p}{}_{j}(d)$ and the obtained regression line through least square fitting for each frequency band. At the distance of 1000 mm, a plot of green circle that denotes the path loss in free space is shown as a reference. The results show that the path loss caused by the presence of the human body often reaches 25 dB in the anechoic chamber. In the hospital room, where there are reflections from the walls and so on, the path loss due to the human body is less than 10 dB. The parameters for the path loss model, which are derived from the measured data, are summarized in Table 3. By substituting the values for each band into the Eq.(2), the path loss for the distance d is obtained. Note that the distance should be more than 100 mm we did not obtain results at distance of less than 100 mm.

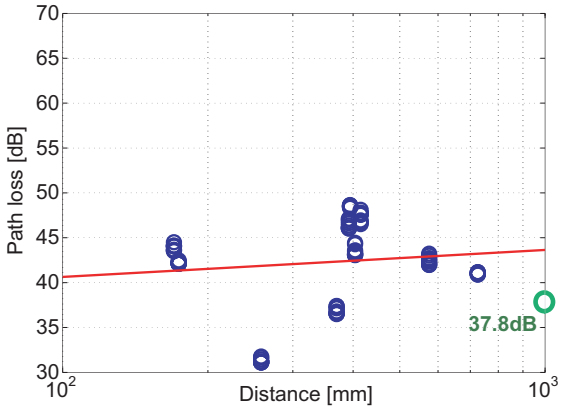

(a) 400 MHz

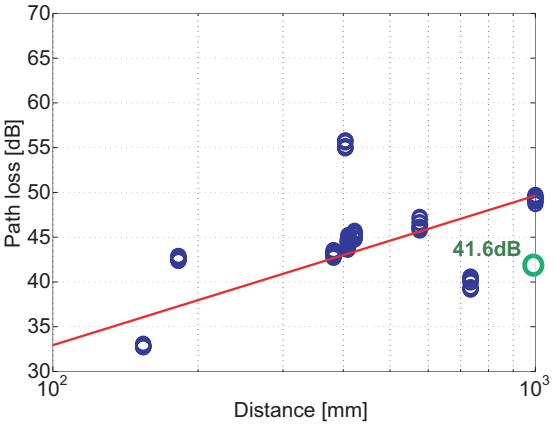

(b) 600 MHz

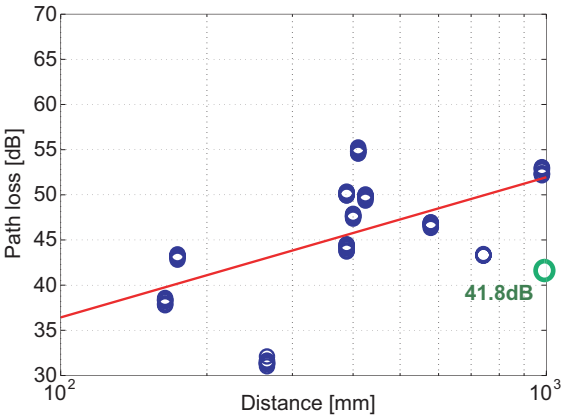

(c) 900 MHz

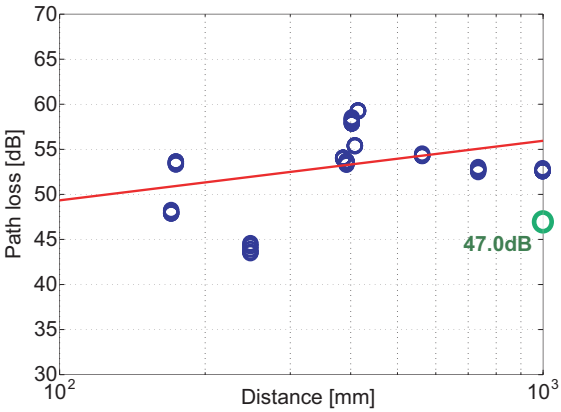

(d) 2.4 GHz

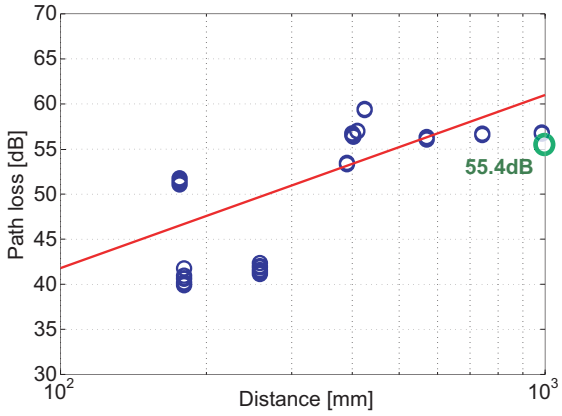

(e) UWB

(1) Hospital room

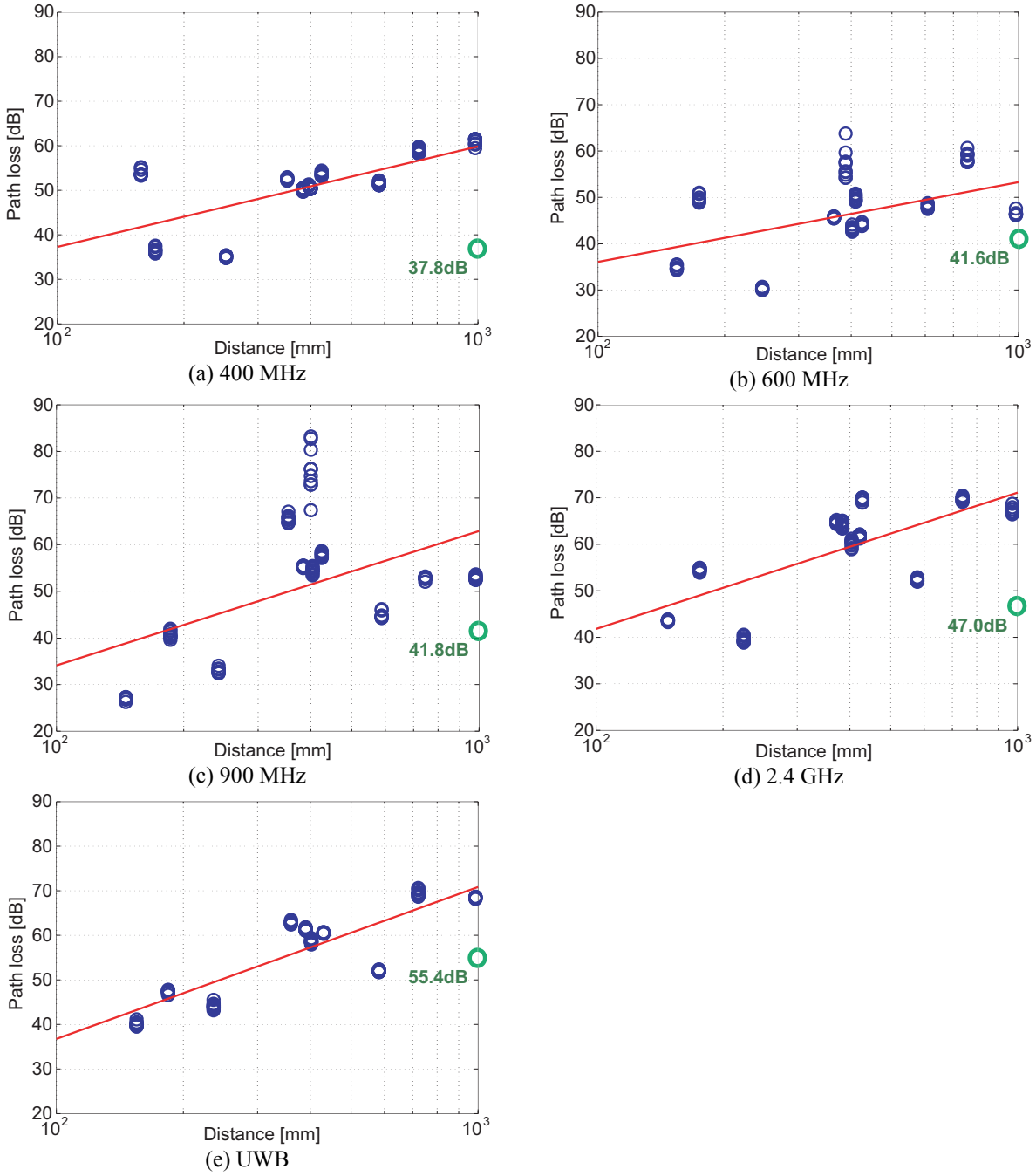

(a) 400 MHz

(b) 600 MHz

(c) 900 MHz

(d) 2.4 GHz

(e) UWB

(2) Anechoic chamber

Figure 3: Path loss models in a hospital room and anechoic chamber for 400, 600, 900 MHz and 2.4 GHz and UWB band.

Table 3: Parameters of path loss models for 400, 600, and 900 MHz, 2.4GHz and UWB band

(a) Hospital room

Parameters	Values				
	400 MHz	600 MHz	900 MHz	2.4 GHz	UWB
a	3.00	16.7	15.5	6.60	19.2
b	34.6	-0.45	5.38	36.1	3.38
σ_N [dB]	4.63	5.99	5.35	3.80	4.40

(b) Anechoic chamber

Parameters	Values				
	400 MHz	600 MHz	900 MHz	2.4 GHz	UWB
a	22.6	17.2	28.8	29.3	34.1
b	-7.85	1.61	-23.5	-16.8	-31.4
σ_N [dB]	5.60	6.96	11.7	6.89	4.85

3.3 Power delay profile model

As shown in Appendix A, highly frequency-selective channels are observed in the UWB band. So, a power delay profile (PDP) model is required to evaluate its performance.
Firstly, Post-processing of the measurement data for the UWB is carried out for deriving the PDP model. The procedure of the post-processing can be summarized as follows. First, Frequency domain windowing was applied prior to the transformation of the frequency domain data to the time domain data. The Hamming window is chosen since it has side lobe suppression about 41 dB. Then, the windowed CTFs were transformed into the channel impulse responses (CIRs) through inverse Fourier transform. Local peaks in each CIR are identified to use only the best paths for channel modeling. Further, a threshold value that is 20 dB less than the amplitude of the strongest path is applied to the obtained local peaks. The CIRs are then normalized such that the amplitude of the first path in each PDP is equal to one. And, the initial delay for each of the transmission links was extracted from the PDP so that all PDPs are aligned with the first path arrives at 0 ns.
The channel model of the PDP is modeled by

$$h(t) = \sum_{l=0}^{L-1} a_l \exp(j\phi_l)\delta(t - t_l) \quad (4)$$

where a_l, t_l, and ϕ_l denote the path amplitude, path arrival time, and phase for the l-th path, respectively. L is the number of the arrival paths, and $\delta(t)$ stands for the Dirac function. The phase ϕ_l is modeled by a uniform distribution over $[0,2\pi)$. The path amplitude a_l is modeled by an exponential decay Γ with a Rician factor γ_0, which is written by

$$10\log_{10}|a_l|^2 = \begin{cases} 0 & l = 0 \\ \gamma_0 + 10\log_{10}\left(\exp\left(-\frac{t_l}{\Gamma}\right)\right) + S & l \neq 0 \end{cases} \quad (5)$$

where and S means a stochastic term modeled by a log-normal distribution with zero-mean and standard deviation of σ_S. The path arrival time t_l is modeled by Poisson distribution, which is given by

$$p(t_l|t_{l-1}) = \lambda \exp(-\lambda(t_l - t_{l-1})) \quad (6)$$

where λ means path arrival rate. And, the number of the arrival paths L is modeled by Poisson distribution, which is written by

$$p(L) = \frac{\bar{L}^L \exp(\bar{L})}{L!} \quad (7)$$

where $\bar{L}$ means the average of the L.

First, the parameters related to the path amplitude a_l are derived from the measured data. All path amplitudes plotted in Fig. 6(a) are expressed in dB; a regression curve obtained through least squares fitting is also plotted in this figure. The values of γ_0 and Γ are derived from the fitted curve, as shown in Table 4. In this table, the values of the parameters derived from the data measured in the anechoic chamber are also provided for reference. The standard deviation σ_S of the stochastic term S is derived by the log-normal fitting among differences between the measured data and the regression shown in Figure 6(b). The parameter λ is obtained from the cumulative density function on t_l-t_{l-1}, as shown in Figure 6(c); here t_l is the arrival time. The fitted result is λ = 1.85 ns. Further, $\bar{L}$ is obtained from the histogram of the number of arrival paths, plotted in Figure 6(d).

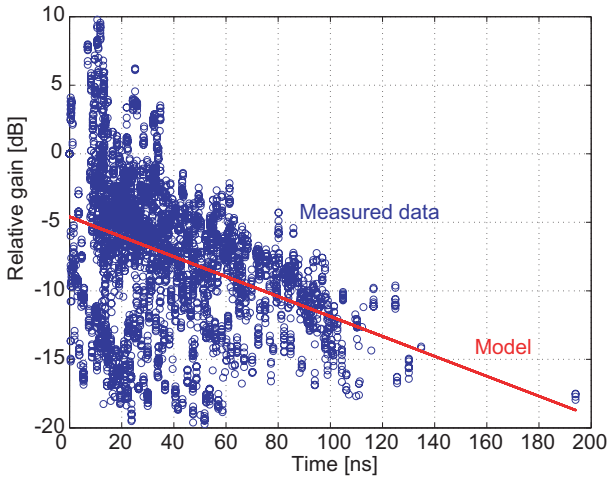

(a) Exponential decay Γ and Rice factor γ_0

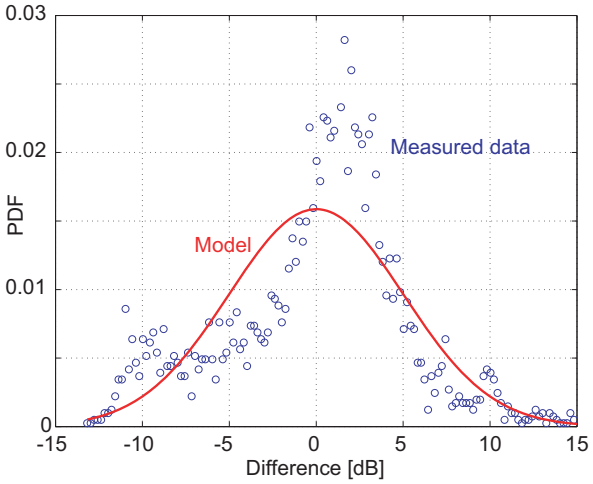

(b) Lognormal standard deviation σ_S

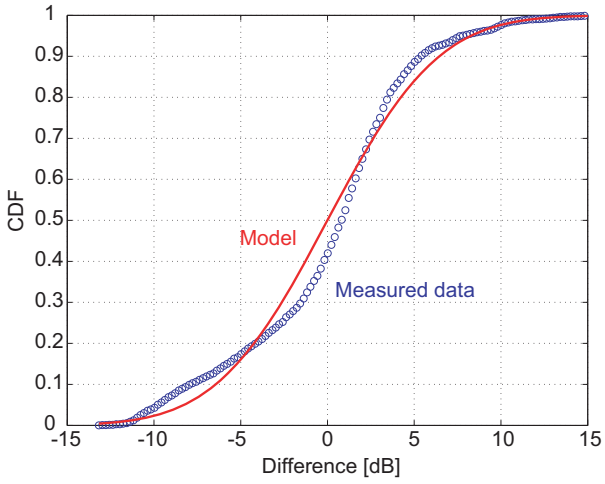

(c) CDF of the lognormal standard deviation σ_S

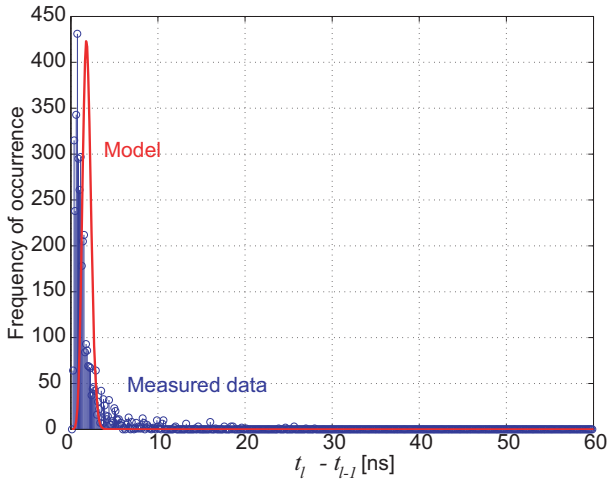

(d) Ray arrival time difference with Poisson distribution with average λ

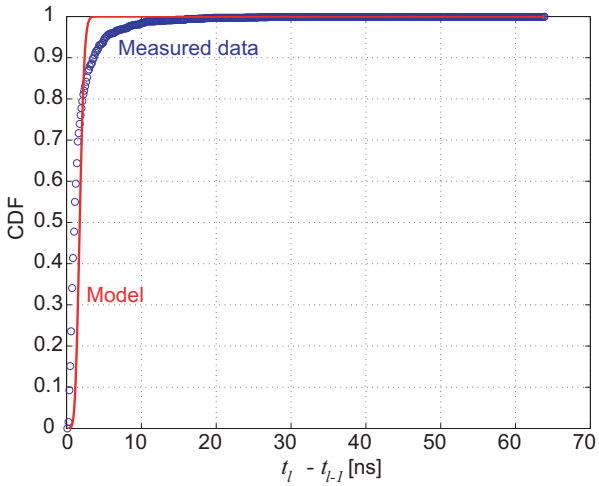

(e) CDF of the ray arrival time difference

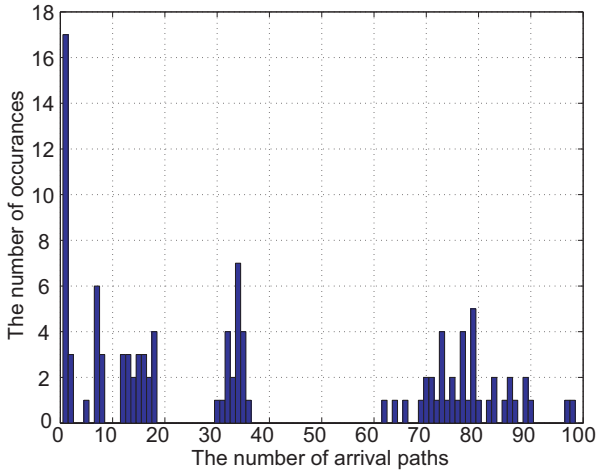

(f) Histogram of the number of arrival paths

Figure 6: Parameters for power delay channel model for UWB band.

Table 4: Parameters' values for the power delay profile model in the hospital room.

Parameters		Values
a_l	γ_0	-4.60 dB
	Γ	59.7
	σ_S	5.02 dB
t_l	λ	1.85 ns
L	$\overline{L}$	38.1

3. Channel model CM4 (UWB band)

3.1 Introduction

At the proximity of the human body, there is a strong interaction of the electromagnetic field between the antenna and the human body. Therefore, the characteristic of the antenna becomes important for BAN channel [5]. Since the transmitter is attached on body, the antenna characteristics will be changed unavoidably. The channel model of 15.4a considered infinitesimally small electric dipole in the simulation and the absolute path gain was calibrated by a commercial UWB antenna. Therefore, the channel model did not consider the more complicated behavior of the antenna - human body interaction.

In this report a BAN channel model between body surface and wireless access point using UWB frequency band (3.1 - 10.6 GHz) is presented. We examine antenna characteristics on human body and measure the propagation characteristics to develop the channel model in office environment. Both line-of-sight and non-line-of-sight situations are considered in measurement,

because human body may turn around in the real scenario. The channel model is assumed as a single cluster model with K-factor. Parameter of the model is extracted by statistical analysis.

3.2 Antenna characteristics on body

Antenna characteristic on body was measured in anechoic chamber. Configuration of the measurement is shown in Fig.7. For antenna pattern measurement in far field, distance between antennas was 6 m, and height of antennas was 2 m. We used vertically polarized omni-directional antennas for both Tx and Rx at UWB frequency band. Tx antenna was teardrop type wideband monopole antenna [6]. Planar UWB antenna (SkyCross SMT-3TO10M-A) has been selected for Rx side, since flat type antenna is better for attaching to the body surface. Fig.8 shows the attached Rx antenna on body. The antenna was fixed at the center of body.
For evaluating of human body effects, antenna pattern without human body is shown in Fig.9. Antenna pattern in H-plane was omni-directional, and the difference of maximum- and minimum-gain was 10dB. Antenna patterns on body are shown in Fig.10. We measured a few antenna patterns by changing the gap between antenna and body. Antenna pattern of front side was almost same as omni-directional, however, the gain of backside in 180 degree was decreased about 20dB by shadowing of body. Antenna patterns were only changed within 60 to +60 degree from the center of backside.

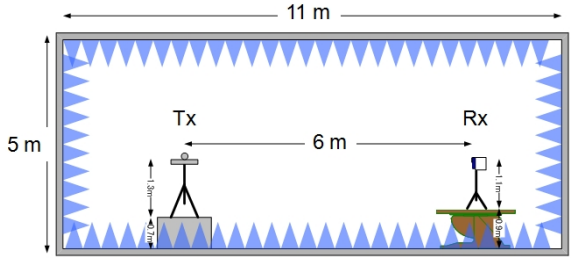

Figure 7: Configuration of antenna measurement

Figure 8: Attached antenna on body.

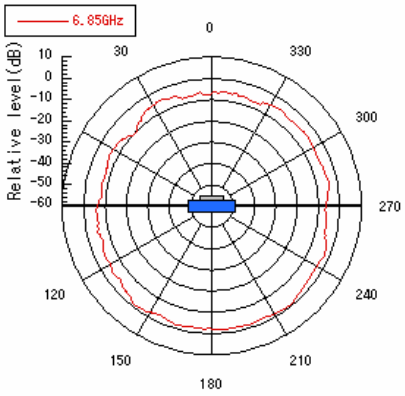

Figure 9: Antenna pattern in air.

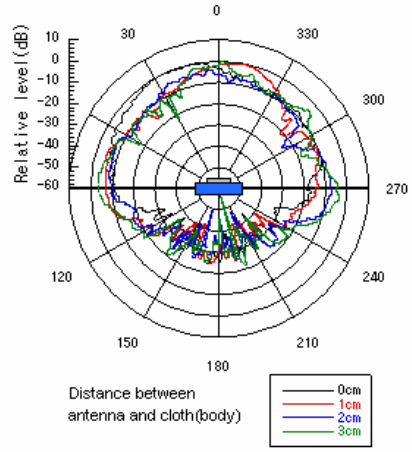

Figure 10: Antenna characteristics on body at 6.85 GHz

3.3 Propagation measurement and analysis

We measure the delay profile by using vector network analyzer. The complex impulse response was calculated from the measured complex transfer function in the frequency domain by FFT function of the instrument. Frequency range was 3.1-10.6 GHz for UWB band. Recently this measurement method is getting major rather than pulse generator and oscilloscope measurement. Measurements were done in office environment for medical health care applications. The room was surrounded by metal walls and windows, and was furnished by desks, chairs and PC monitors, as shown in Fig.11. Floor was made of concrete board covered by carpet. The measurement configuration is shown in Fig.12 with positions of Tx and Rx antennas. Tx position was fixed near the wall, and Rx positions were changed in human movement area. In this

measurement, human direction was also changed for considering shadowing by human body. Rx antenna on body was aligned to Tx antenna at 0 degree as in the geometry of Fig.12.
Impulse responses are shown in Figs.13 in case of three body directions. In 0 degree case (Fig.13a), the direct path component can be seen as the first impulse response, and other multi-path responses became a cluster. On the other hand, in side (Fig.13b) and backside (Fig.13c) cases, the direct path components were attenuated and vanishing respectively. Thus only one cluster can be seen in both cases.
For PHY layer simulation in wide band system design, statistical channel model is often used. Since the statistical channel model can generate various channel realizations with some parameter, the system performance as bit error rate (BER) can be estimated by using the model. To obtain the channel model parameters, the ray information of measured data was required. In this report, CLEAN algorithm was used to extract the ray information from measurement data [7]. This algorithm is based on a peak detection method, and was used in some previous researches. The response of the ray extracted from all the measurement data is shown in Fig.14. We considered the effect of ground in our measurements. However, all data were averaged for statically analysis. Hence; the detail data of each measurement is not described. Since transmission distance is different for each Rx position, all responses were normalized by the maximum value, and the delay time of the first response was shifted to 0. From these figures, the cluster decay factor Γ was estimated by regression line in each body direction. Then the effect of K-factor k was also estimated by the difference of averaged first response level. Another parameter, the lognormal standard deviation σ of normalized ray amplitude was estimated by curve fitting as shown in Fig.15.

(a) View from wall side.

(b)View from window side.

Figure 11: Measurement room

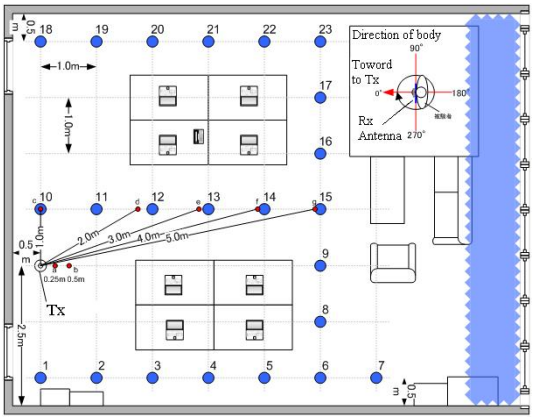

Figure 12: Configuration of propagation model for UWB band

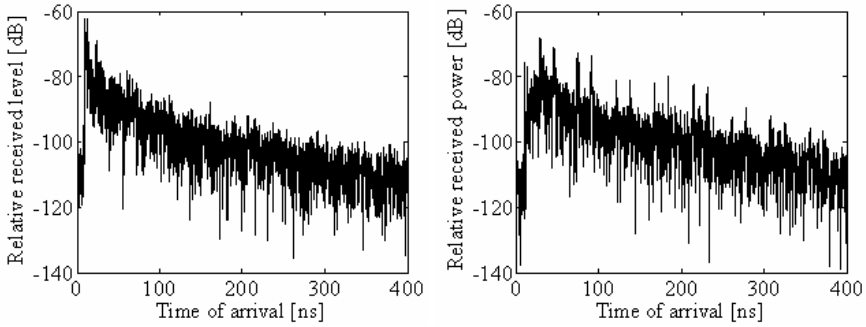

(a) θ = 0 deg (Front of body). (b) θ = 90 deg (Side of body).

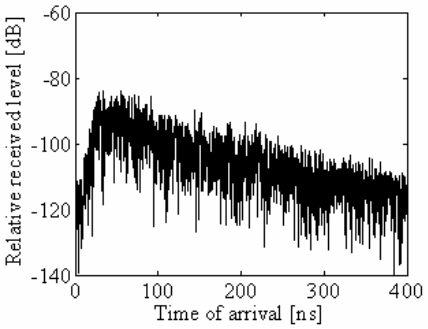

(c) θ = 180 deg (Backside of body).

Figure 13: Example delay profile for each channel position

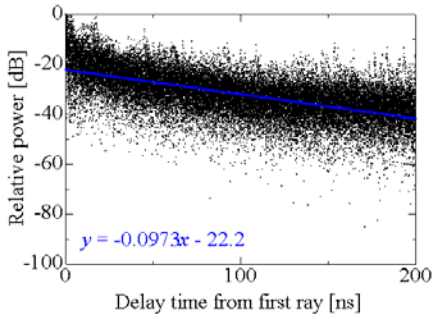

(a) θ = 0 deg (Front of body).

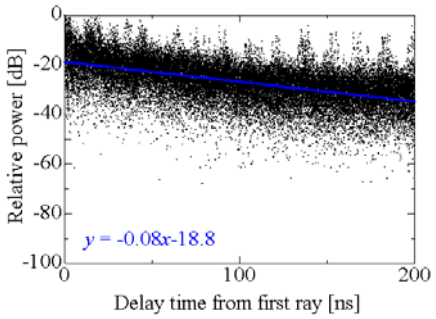

(b) θ= 90 deg (Side of body).

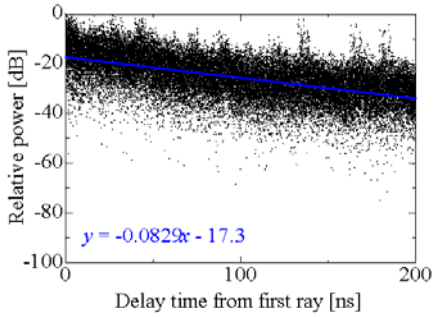

(c) θ= 270 deg (Side of body).

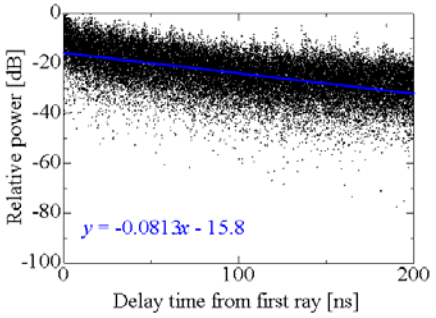

(d) θ = 180 deg (Backside of body).

Figure 14: Statistical analysis of delay components for each body position

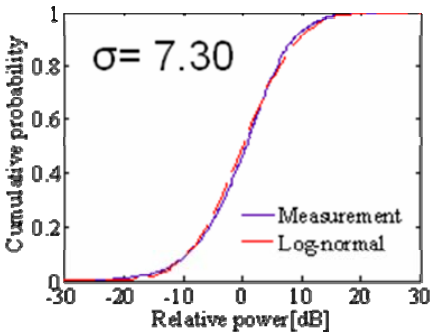

(a) θ= 0 deg (Front of body).

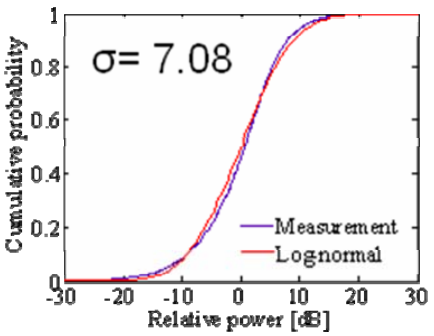

(b) θ = 90 deg (Side of body).

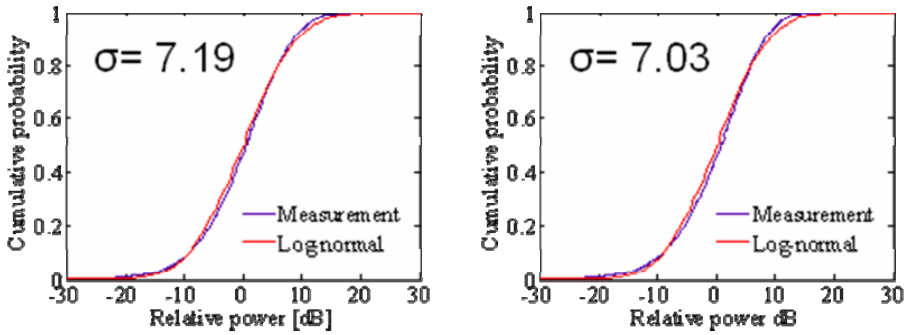

(c) θ = 270 deg (Side of body). (d) θ = 180 deg (Backside of body).

Figure 15: CDF of delay components.

3.4 Channel model

From results of Section 3.3, we assumed the one cluster with direct path component as a generic BAN channel model for both line-of-sight and non-line-of-sight situations. The equation of the model is expressed as follows.

$$h(t) = \sum_{m=0}^{\infty} \alpha_m \delta(t - \tau_m) \quad (8)$$

$$\overline{|\alpha_m|^2} = \Omega_0 e^{-\tau_m/\Gamma - k[1-\delta(m)]} \quad (9)$$

$$\angle \alpha_m \propto \text{Uniform}[0, 2\pi) \quad (10)$$

Here $h(t)$ is complex impulse response, m is number of the ray, a_m is the amplitude of each ray, τ_m is a sampling rate of system, the phase of each ray is assumed as random, and k as the effect of K-factor is included [8]. The path loss Ω_0 depends on the environment and line-of-sight situation. In this report, the value of Ω_0 can be calculated by adding the intercept value in Y-axis of Fig.14a to path loss of direct path for line-of sight situation. For non-line-of-sight situation, k was already considered in Eq.8 for including path loss effect. The effect k is calculated by the difference (Δk) of averaged first impulse responses in Fig.14. Relationship of Δk and k is shown as

$$k = \Delta k(\ln 10/10) \quad (11).$$

The channel response which is obtained by Eq.8 is shown in Fig.16. For line-of-sight situation, τ_0 can be calculated by following equation.

$$\tau_0 = d / c \quad (12)$$

Here d is transmission distance, and c is light wave speed. For non-line-of-sight situation, τ_0 is assumed as random. Model parameters were calculated by statistical analysis in Section 3.3. Parameter set is shown in Table 5.

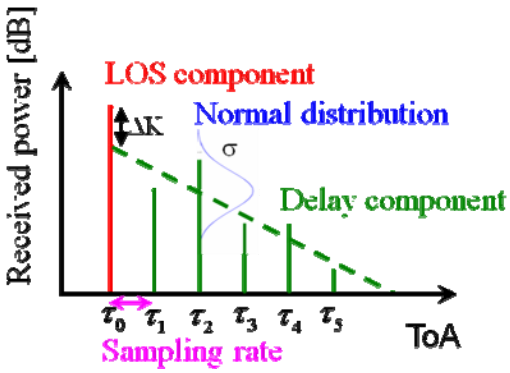

Figure 16: Channel model of one cluster with LOS component.

Table 5: Channel model parameters for each body position

Direction of body	Γ [ns]	k (Δk [dB])	σ [dB]
0	0.224	1.47 (6.4 [dB])	7.30
90	0.184	0.691 (3.0 [dB])	7.08
180	0.187	0 (0 [dB])	7.03
270	0.191	0.345 (1.5 [dB])	7.19

4. Informative reference for CM2

This section provides an informative material useful to develop a channel model CM2.

4.1 Received signal strength analysis by FDTD

A simulation software (SEMCAD) is used to evaluate the received signal level to give useful information for preparing a channel model CM2. In this analysis, FDTD with UPML is used. The measurement frequency is 403.5 MHz, which is in the MICS band. A 100-MHz wide pulse is inputted. Outside antenna is a half-wave length dipole. Implanted antenna is modeled by a 5-mm line element. A numerical phantom model [10] for a human body is employed. In the analyses, contents of its stomach, small and large intestines are modeled as electrical constants of either air or muscle. The analyses are carried out for 15 positions of the implanted element as listed in Fig. 17.

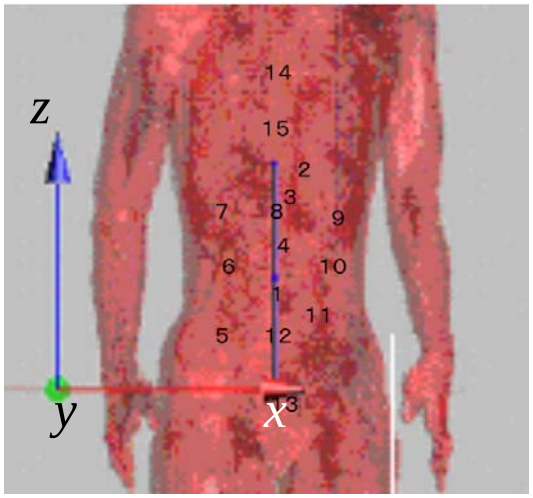

1	Transmitting antenna (on body)
2	Stomach
3	Duodenum
4	Small intestine
5	Large intestine 1
6	Large intestine 2
7	Large intestine 3
8	Large intestine 4
9	Large intestine 5
10	Large intestine 6
11	Large intestine 7
12	Large intestine 8
13	Large intestine 9
14	Oesophagus 1
15	Oesophagus 2

Figure 17: Positions of the implanted element in the FDTD analyses.

Conditions in the simulation are as follows. UPML(Uniaxial Perfect Matching Layer) is applied into its boundary. Cell size of a numerical phantom is 2 mm x 2 mm x 2 mm. Its spatial volume of the numerical phantom model is 450 mm x 600 mm x 590 mm. Then, this phantom model is divided into 85 Mcells.
Its VSWR of the dipole antenna, which is the outside antenna, for both on-body and free-space are shown in Fig. 18. In the free-space condition, VSWR is less than 1.5 at 403.5 MHz. On the

other hand, in the case of on-body condition, its resonance frequency is shifted to around 393 MHz due to the effect of the human body. The VSWR in minimum is 1.2.

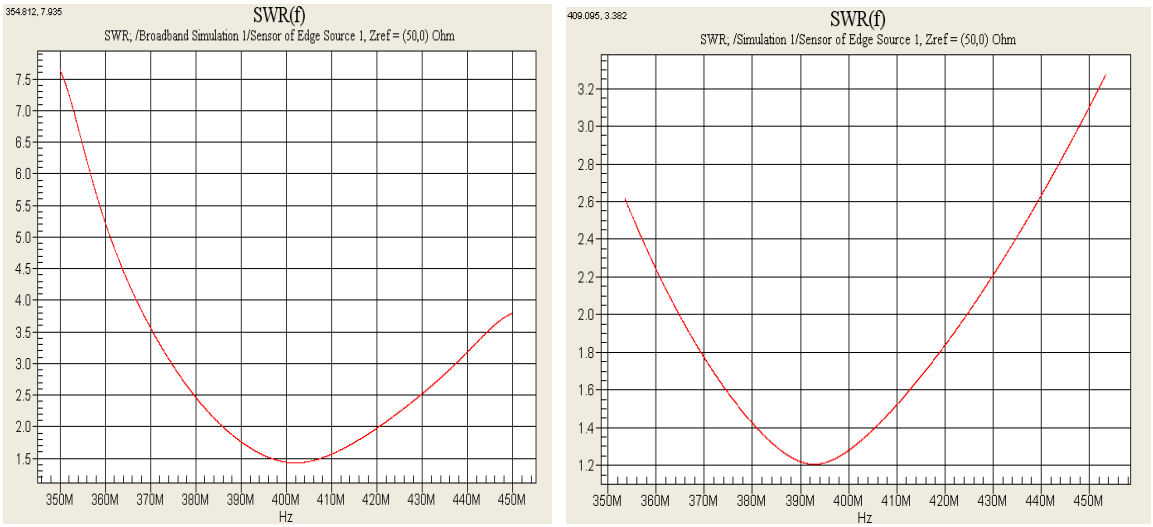

(a) free-space condition (b) body-worn condition

Figure 18: VSWR of the dipole antenna for 403.5 MHz.

The obtained received signal levels, which are relative values to the input signal level, are shown in Fig. 19. In these results, x, y, and z level means the received signal levels along its x, y, and x axes shown in Fig. 17. From the obtained results, a path loss model is derived for implant channel at 400-MHz band. A path loss model that is derived by a least square fitting is shown in Fig. 20. The path loss model under co-polarization is given. The slope of the path loss model is -1.93 dB/cm.

	x level [dB]	y level [dB]	z level [dB]
Mean	-72.10	-69.82	-54.18
Stddev.	14.08	11.75	13.24
Maximum	-55.54	-43.23	-38.18
Minimum	-115.41	-95.04	-79.66
Fluct.	59.86	51.82	41.48

(a) Received signal level for each position of in-body (Contents of the stomach, small and large intestine are assumed to be muscle)

	x (air) level [dB]	y (air) level [dB]	z (air) level [dB]
Mean	-75.09	-73.50	-56.77
Stddev.	13.92	8.50	13.68
Maximum	-57.56	-57.92	-38.18
Minimum	-112.47	-92.96	-82.69
Fluct.	54.91	35.04	44.51

(a) Received signal level for each position of in-body (Contents of the stomach, small and large intestine are assumed to be air)

Figure 19: VSWR of the dipole antenna (403.5 MHz).

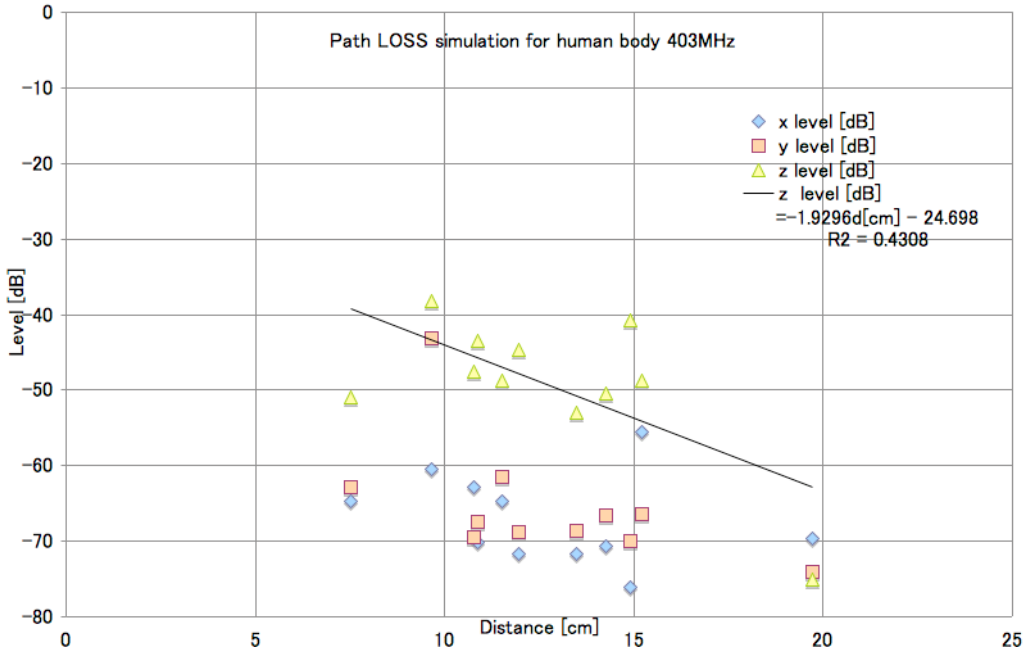

Figure 20: Path loss model for the 400-MHz band implant scenario. This model is obtained by least square fitting for the co-polarization (z-level) component. Its path loss slope has -1.93 dB/cm.

The received signal levels corresponding to the 14 positions of the human phantom model are evaluated through FDTD analyses. The results shown in Figure 9 demonstrate that:

- The received signal level under the co-polarization is around -54 dB.
- The difference of the signal level between the co- and cross-polarization is around 17 dB.
- The impact of the contents of the stomach and intestines on its received signal levels are slight.
- The slope of the path loss model for co-polarization condition is -1.93 dB/cm.

4.2 Experimental measurement

This experiment is conducted to confirm the results obtained by FDTD analyses in the previous section 4.1. First, measurement results on received signal levels are shown under an experimental setup. Then, results obtained by the FDTD analysis as same as the previous section are shown. In this experiment, a liquid phantom is used. Its complex permittivity of the liquid phantom is 42.3 and 39.4 in real and imaginary parts, respectively.
Figure 21 shows the outlook of its signal generator and experiment setup. The size of the signal generator is around 10 mm x 10 mm x 20 mm. Its oscillation frequency is 403 MHz. This signal generator is set at inside of the liquid phantom. A cylinder is prepared to contain the liquid

phantom, and its diameter is 150 mm and its height is 300 mm. We prepare 3 types of antenna, a dipole, chip, and skeleton-slot, which is settled at the outside of the cylinder. Its separation between the antenna and cylinder is set to 15 mm. The outlook of the antennas is shown in Fig. 22. In this experiment, its signal levels at the outside antennas are measured by a spectrum analyzer, as the position of the signal generator is changed in the liquid phantom. This measurement was carried out in an anechoic chamber. The signal generator is set at the distance of {50, 70, 90, 110, 130, and 150 mm} from the cylinder wall that is the closest side for the received antenna. This distance is denoted as d_1. In this measurement, the preamp with 40-dB gain is inserted.

(a) Signal generator for 403 MHz

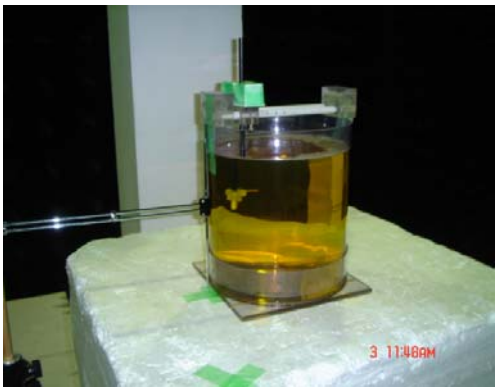

(b) Experiment setup (the yellow liquid is the liqud phantom)

Figure 21: Outlook of the signal generator and experimental setup in an anechoic chamber.

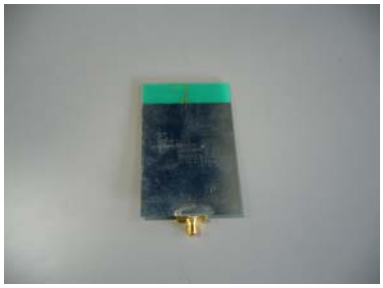

(a) Chip antenna

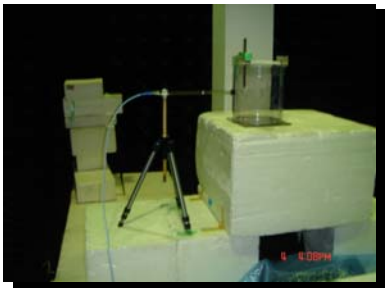

(b) dipole antenna (Anritsu MP663A)

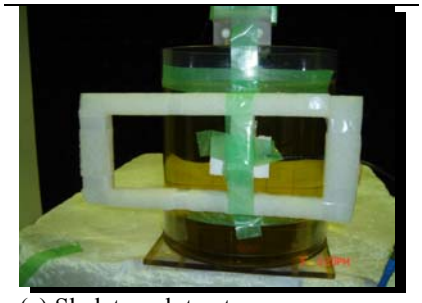

(c) Skeleton-slot antenna

Figure 22: Outlook of the antennas for this measurement.

The measurement results are shown in Fig. 23 (a). This result shows that the liquid phantom increases the path loss and the type of the antenna has impact on its received signal level. The path attenuation coefficient for the antennas is around 2. Fig. 23 (b) shows that results obtained through FDTD analysis by using SEMCAD-X. In this simulation, the experiment setup when the dipole antenna is used as the received antenna is modeled. The analyzed result shows that the

path attenuation is -2.2, which agrees with the results obtained by measurement result shown in Fig. 22(a). This agreement supports the obtained results through FDTD analysis by using the SEMCAD-X. In the section 4.1, the slope of the path loss, which is derived from the human phantom model, is -2.3 dB/cm for the half-wavelength dipole antenna. The results shown in Fig. 23(a) says that the slope is -2.089 dB/cm; These results show good agreement between measured and simulated results.

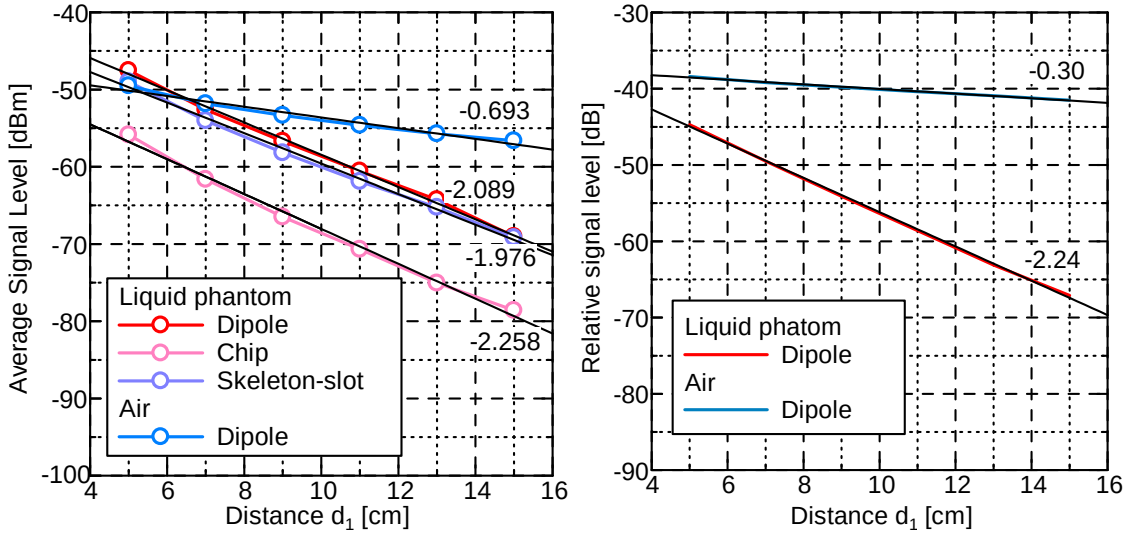

(a) experiment results (b) FDTD analysis

Figure 23: Measurement results of the received signal levels under a liquid phantom for the frequency of 403 MHz.

4.3 Path loss model

The obtained path loss models through simulation and experiments are based on a linear model. However, in actual implanted channels, there is a fluctuation on its received signal level due to the organ structure. This fluctuation for the human body phantom is evaluated by using SEMCAD. Its path loss fluctuation corresponding to its antenna angle between Tx and Rx ones are obtained. The antenna angle parameter $P(\theta)$ [dB] and the fluctuation N, which has Gaussian distribution with zero-mean and standard deviation of σ_N[dB], are introduced into their path loss model for the Implantable BAN, say

$$\mathrm{PL}(d,\theta) = a \cdot d + b + P(\theta) + N \ \ [\mathrm{dB}] \quad (13)$$

where, a and b are path loss coefficients; a is distance slope obtained by vessel simulation and b is a reference level obtained by vessel experiment. d denotes the distance (cm), and σ_N means fluctuation in dB, which is derived from human body simulation. And, $P(\theta)$ is given by

$$P(\theta) = 20 \cdot \log_{10}\left(\cos\theta \cdot (1 - x_c) + x_c\right) \ [\mathrm{dB}] \quad (14)$$

where θ is the antenna angle between implanted and outside antennas, which is assumed to be uniformly distributed over [0..π/2], and x_c denotes polarization parameter. These parameters are

derived from obtained results through experiments and simulations. The parameter *a* is derived through the simulation using human electromagnetic constant of averaged muscle (Tx: in-body 5mm line element, Rx: outside body dipole antenna (1.5cm distance). For the 403 MHz case, it shows agreement with real human numerical model simulation). The parameter *b* is also obtained by the simulation (for 403 MHz case, simulation and the experiment result show agreement within 2 dB). The fluctuation of the path loss is obtained as σ_N=6.59 dB, which is calculated through computer simulations. And, x_c= 0.145 (= -16.78 [dB]), which is derived by the real human body simulation. Additionally, if the outside body antenna is replaced from the half-wavelength dipole one to the printed chip antenna, which is used in the experiment, the loss of 6.34 dB need to be included in Eq. (13). This loss is due to the use of the chip antenna instead of the dipole one. The parameters for this path loss model are summarized in Table 5

Table 5: Parameters of the path loss model for implanted WBAN

Parameters	Values
a	1.92
b	39.85
σ_N	6.59
x_c	0.145

Acknowledgement

The authors would like to thank Mr. Hironobu Watanabe and Mr. Fumio Ohkubo who are working with NTT Advanced Technology Corporation.

5. References

[1] K. Y. Yazdandoost, et al., "Channel Model for Body Area Network (BAN)," IEEE 802.15-08-0033-04.

[2] D. Lewis, "802.15.6 Call for Applications - Response Summary," IEEE 802.15-08-0407-02.

[3] H.-B. Li, et al., "IEEE 802.15.6 Regulation Subcommittee Report," IEEE 802.15-08-0034-08.

[4] K. Takizawa, T. Aoyagi, J. Takada, N. Katayama, K. Y. Yazdandoost, T. Kobayashi, R. Kohno, "Channel models for wireless body area networks," Proc. of IEEE EMBC 2008, Aug. 2008.

[5] Peter S. Hall Yang Hao, "Antennas and Propagation for Body-centric Wireless Communications," Artech House Aug.2006

[6] T. Taniguchi and T. Kobayashi,"An omni-directional and low-VSWR antenna for the FCC-approved UWB frequency band," in Proc. IEEE AP-S Int. Symp. AP-S'03, Columbus, OH, Jun. 2003, pp. 460–463.

[7] J.A. Högbom, "Aperture Synthesis with Non-Regular Distribution of Interferometer Baselines", Astronomy and Astrophysics, 15:417, 1974

[8] Hirokazu Sawada, Yozo Shoji, Chang-Soon Choi, "Proposal of Novel Statistic Channel Model for Millimeter-wave WPAN," Proceedings of Asia-Pacific Microwave Conference 2006,

no. FR4D-3, Nov. 2006.
[9] Hirokazu Sawada, Takahiro Aoyagi, Jun-ichi Takada, Kamya Yekeh Yazdandoost, and Ryuji Kohno, "Channel model for wireless body area network," The Second International Symposium on Medical Information and Communication Technology, Dec. 2006.
[10] T. Nagaoka, S. Watanabe, K. Sakurai, E. Kunieda, S. Watanabe, M. Taki and Y. Yamanaka, "Development of Realistic High-Resolution Whole-Body Voxel Models of Japanese Adult Male and Female of Average Height and Weight, and Application of Models to Radio-Frequency Electromagnetic-Field Dosimetry " Physics in Medicine and Biology, Vol.49, pp.1-15, 2004.

Appendix A. Summary of the measured S21

In this measurement campaign, we took 10 snapshots of its channel transfer function, S21, for each frequency band and antenna position. The measurement cites are a hospital room and anechoic chamber. This appendix provides all of the measured S21 as reference. Fig. A.1 shows measurement setup, which is the same as Fig. 1., and Fig. A.2 displays photographs in the measurements.

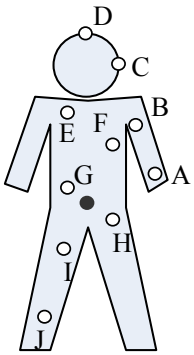

(a) Measurement positions on the human body

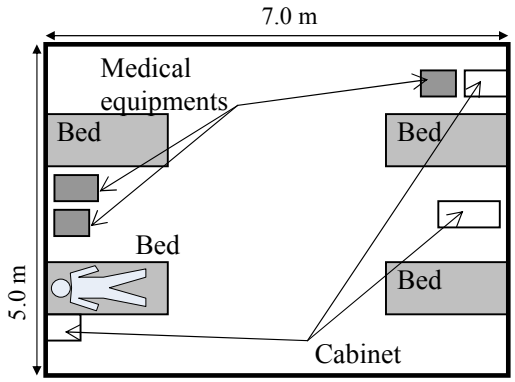

(b) Layout of the measurement room (a hospital room)

Figure A.1 Measurement setup

Figure A.2 Photograph

A. 1 Measurement results in a hospital room
(a) 400MHz band (400 - 450 MHz)

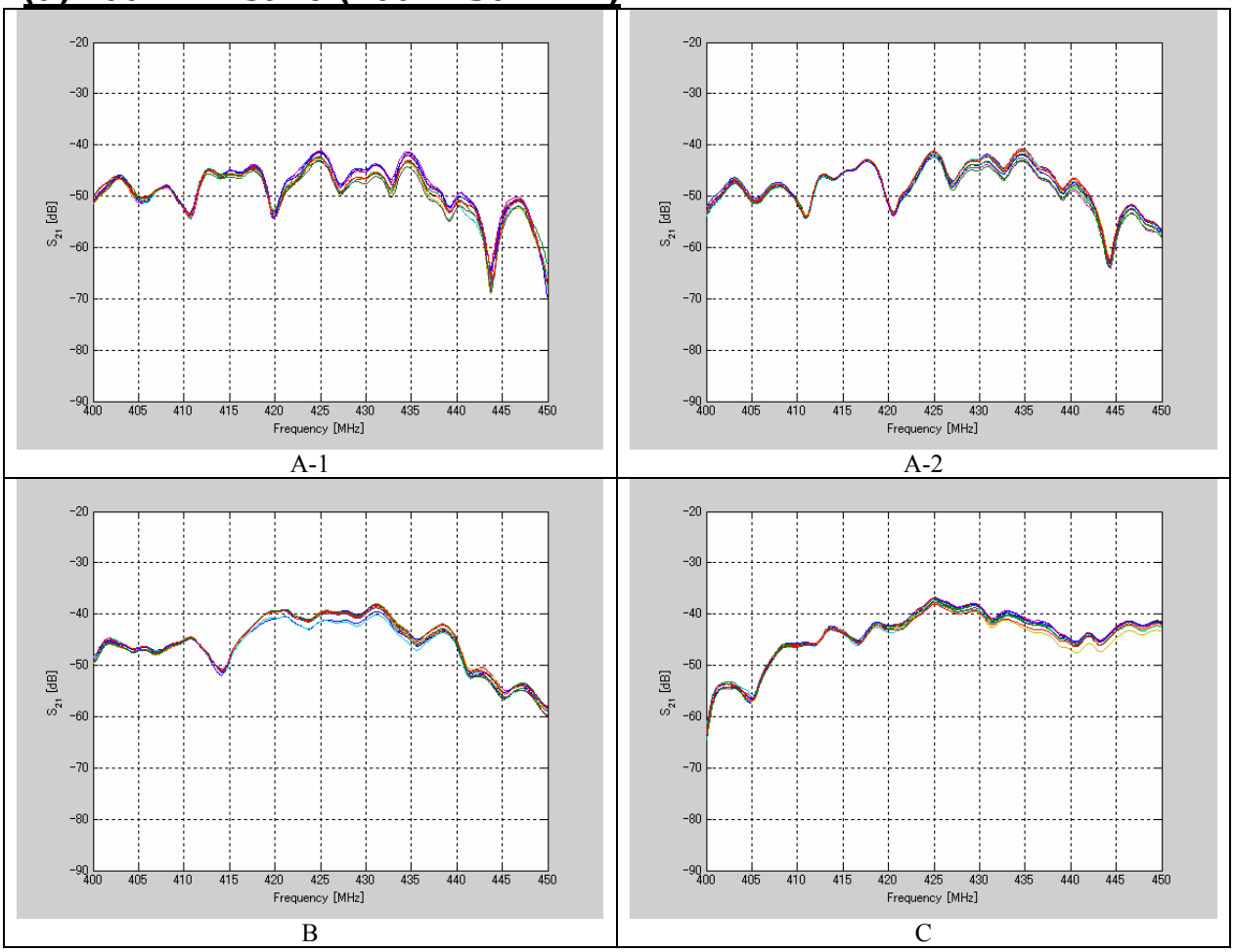

A-1 A-2

B C

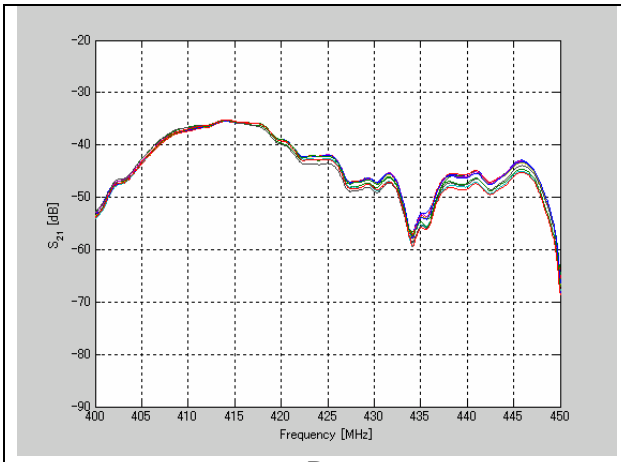
S21 [dB]
Frequency [MHz]

D

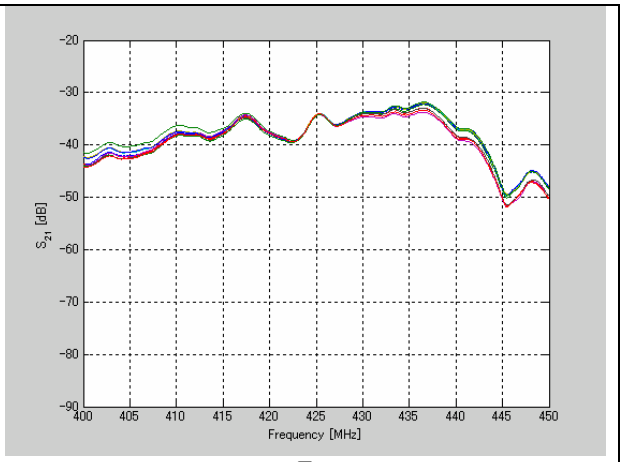
S21 [dB]
Frequency [MHz]

E

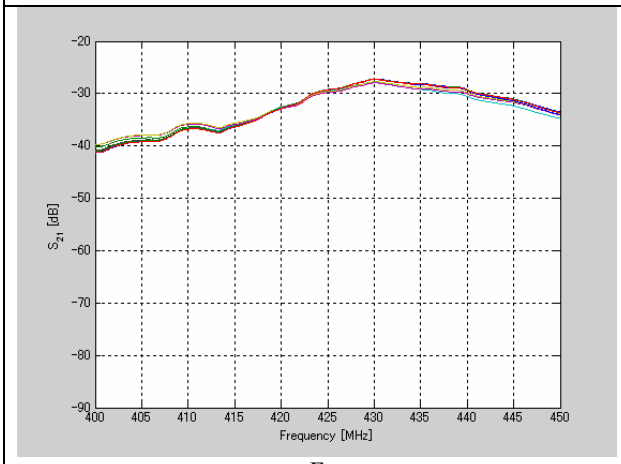
S21 [dB]
Frequency [MHz]

F

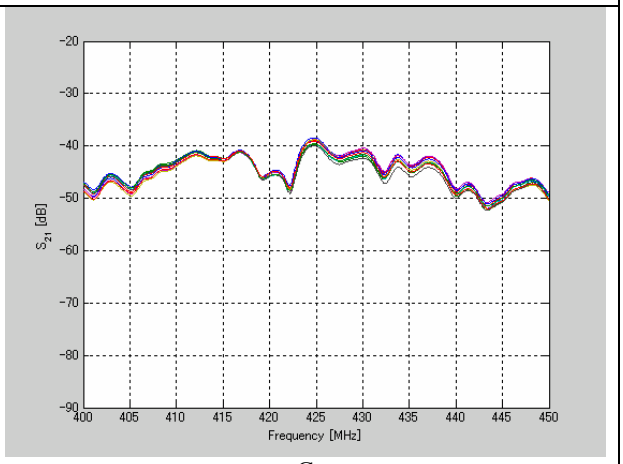
S21 [dB]
Frequency [MHz]

G

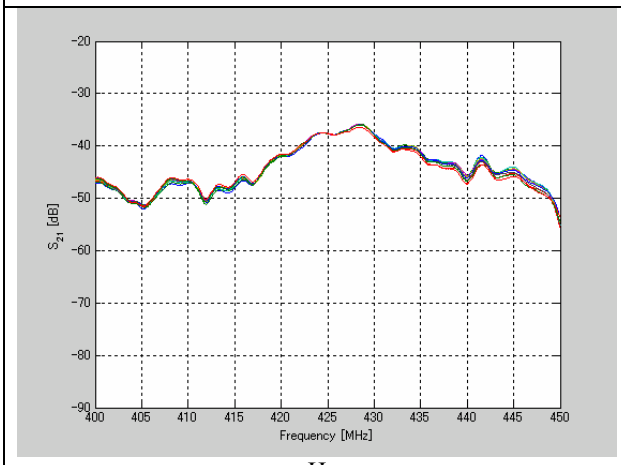
S21 [dB]
Frequency [MHz]

H

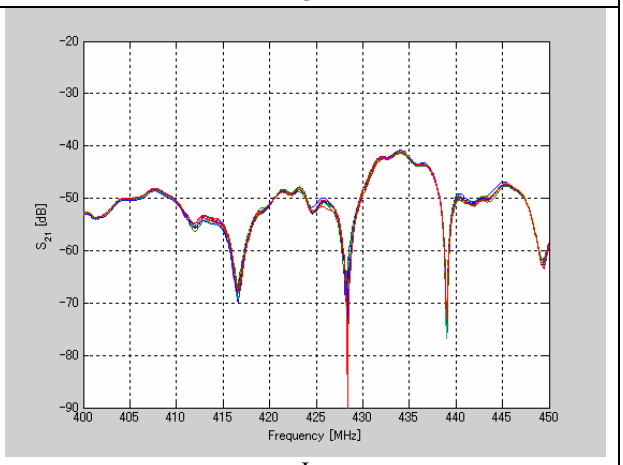
S21 [dB]
Frequency [MHz]

I

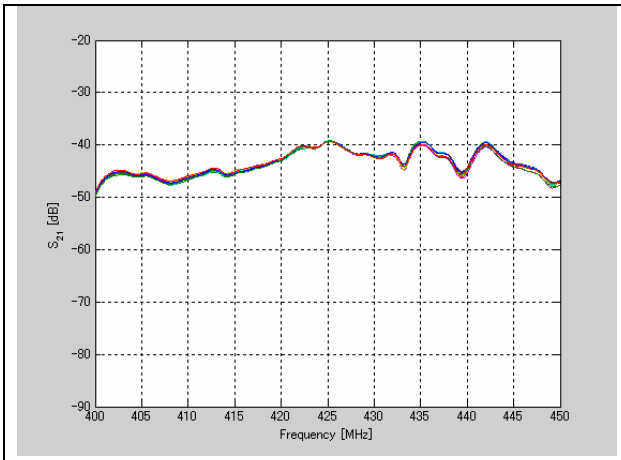

J

(b) 600MHz band (608 - 614 MHz)

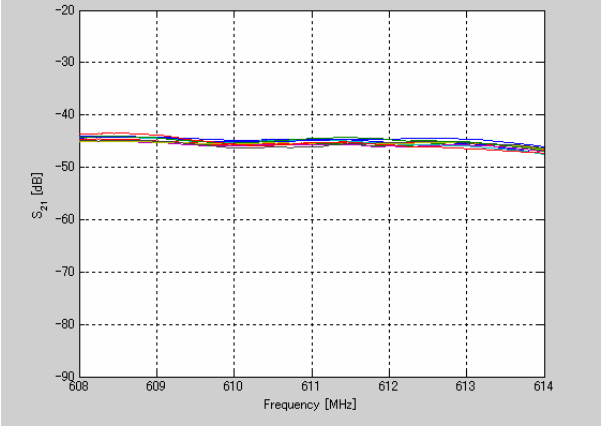

A-1

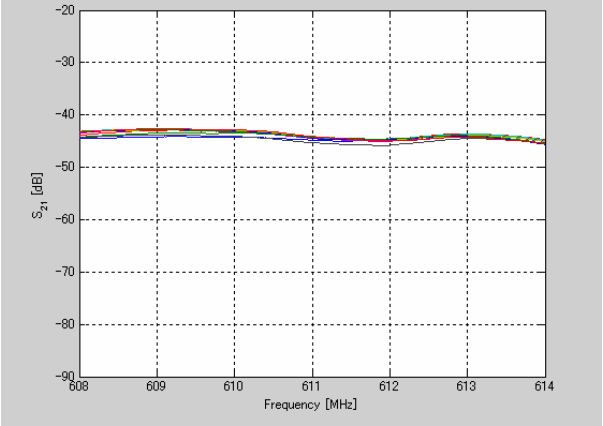

A-2

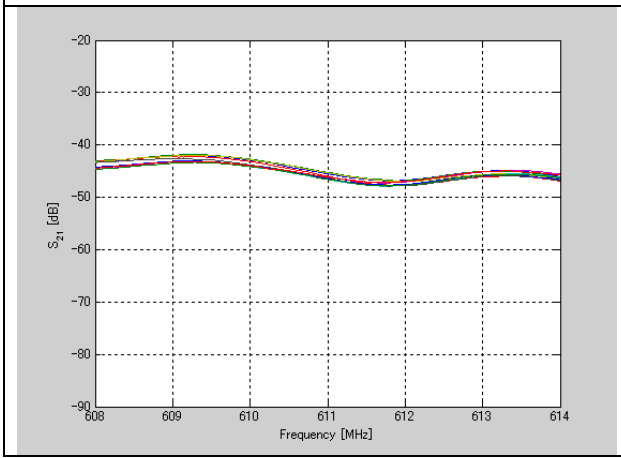

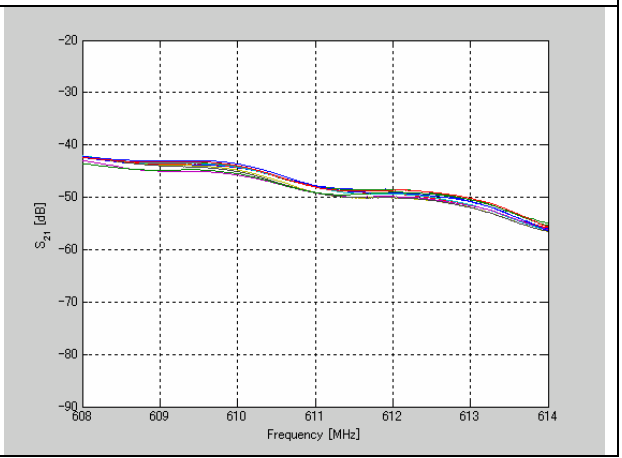

B

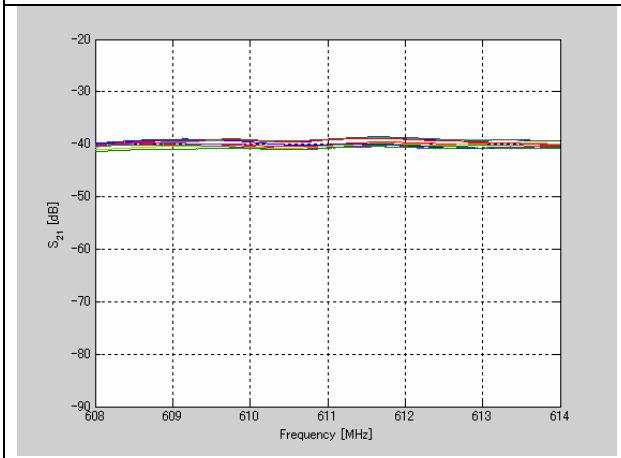
-20
-30
-40
-50
-60
-70
-80
-90
608
609
610
611
612
613
614
Frequency [MHz]
S21 [dB]

C

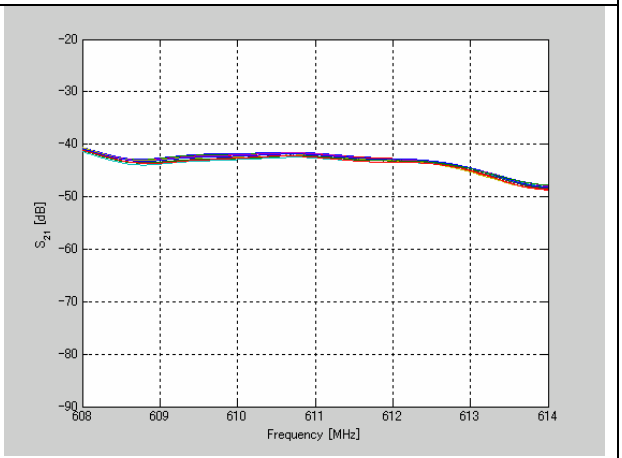
-20
-30
-40
-50
-60
-70
-80
-90
608
609
610
611
612
613
614
Frequency [MHz]
S21 [dB]

D

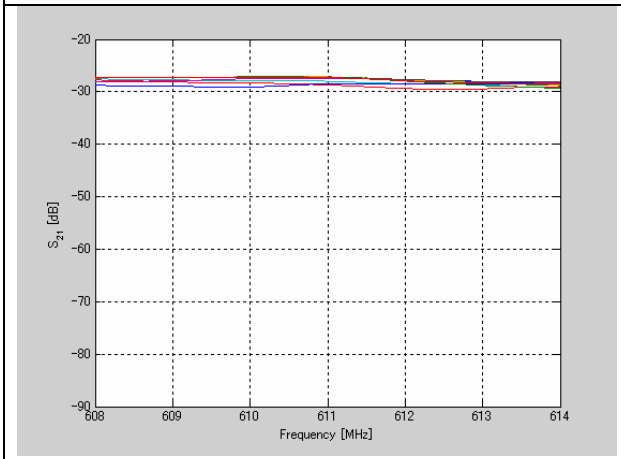
-20
-30
-40
-50
-60
-70
-80
-90
608
609
610
611
612
613
614
Frequency [MHz]
S21 [dB]

E

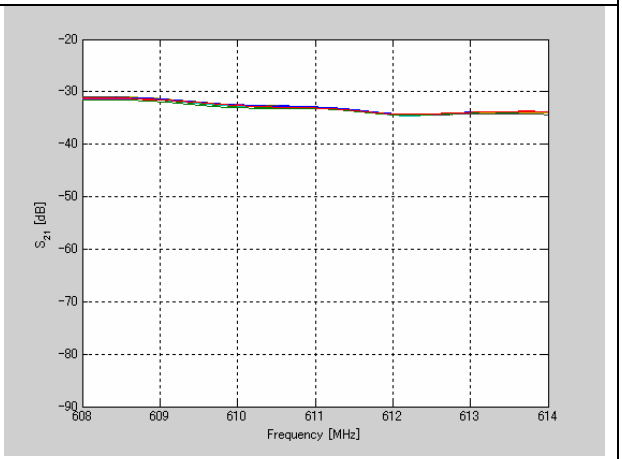
-20
-30
-40
-50
-60
-70
-80
-90
608
609
610
611
612
613
614
Frequency [MHz]
S21 [dB]

F

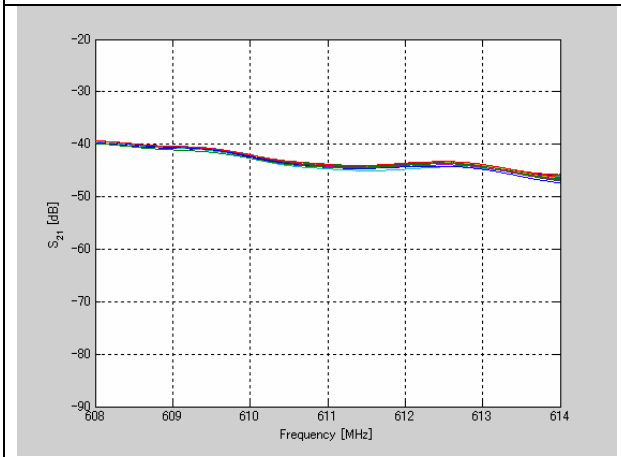
-20
-30
-40
-50
-60
-70
-80
-90
608
609
610
611
612
613
614
Frequency [MHz]
S21 [dB]

G

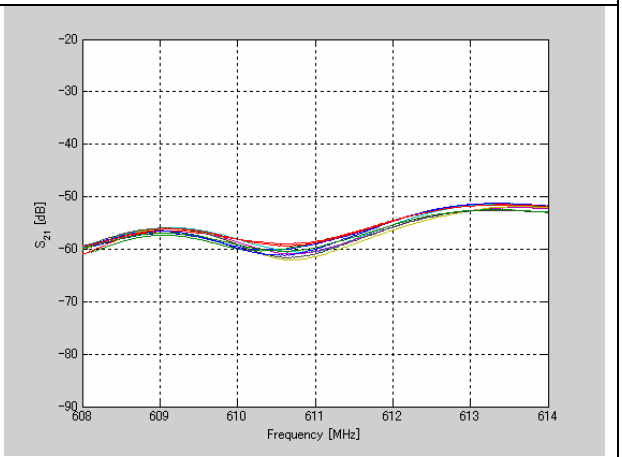
-20
-30
-40
-50
-60
-70
-80
-90
608
609
610
611
612
613
614
Frequency [MHz]
S21 [dB]

H

-20
-30
-40
-50
-60
-70
-80
-90
608
609
610
611
612
613
614
Frequency [MHz]
S21 [dB]

I

-20
-30
-40
-50
-60
-70
-80
-90
608
609
610
611
612
613
614
Frequency [MHz]
S21 [dB]

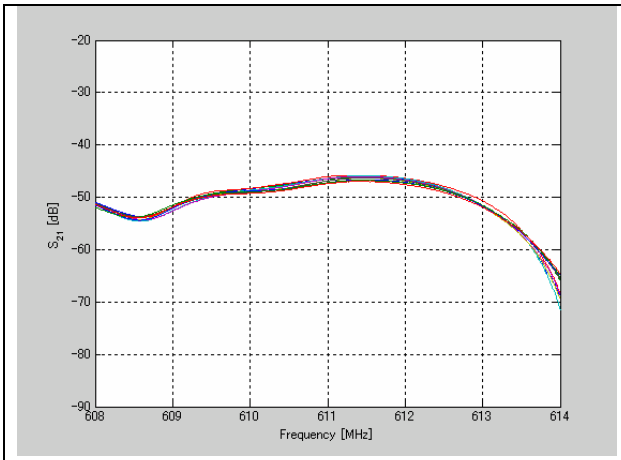

J

(c) 900MHz band (950 - 956 MHz)

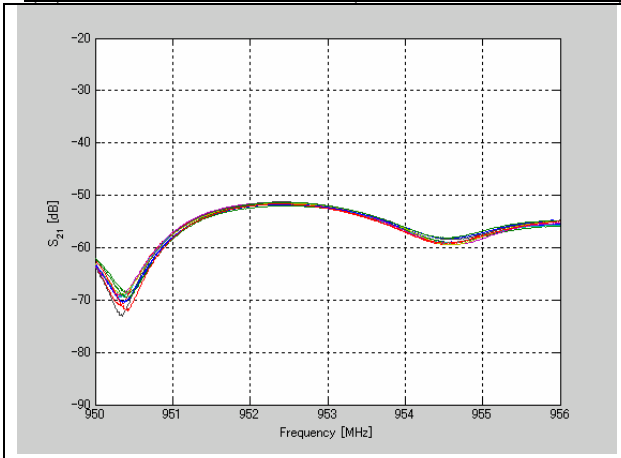

A-1

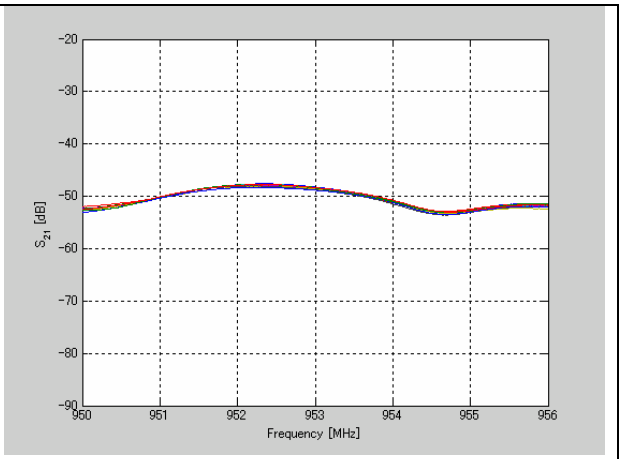

A-2

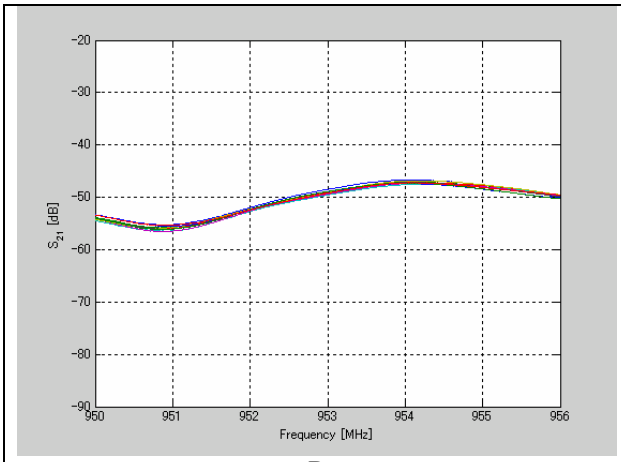
S21 [dB]
Frequency [MHz]

B

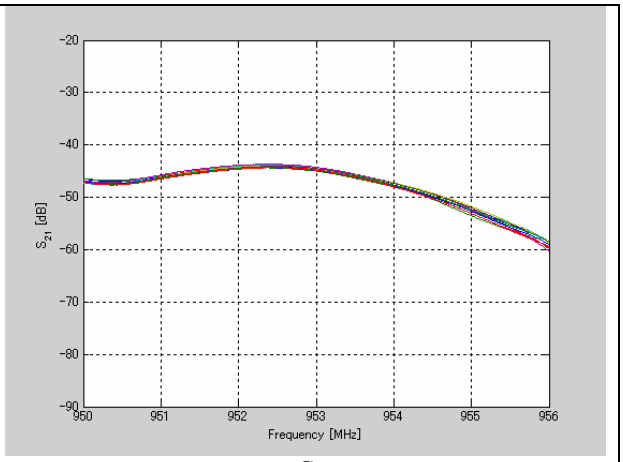
S21 [dB]
Frequency [MHz]

C

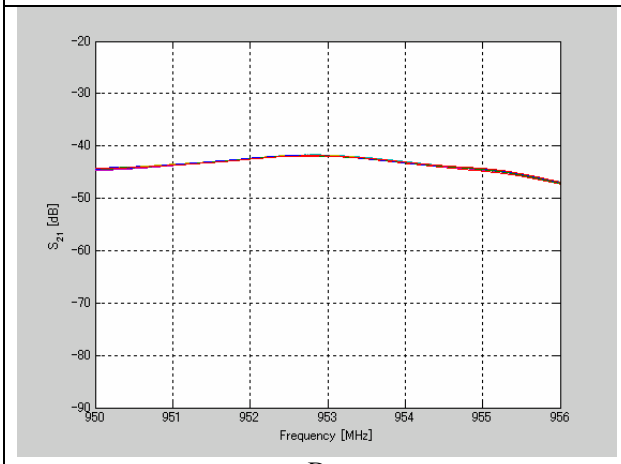
S21 [dB]
Frequency [MHz]

D

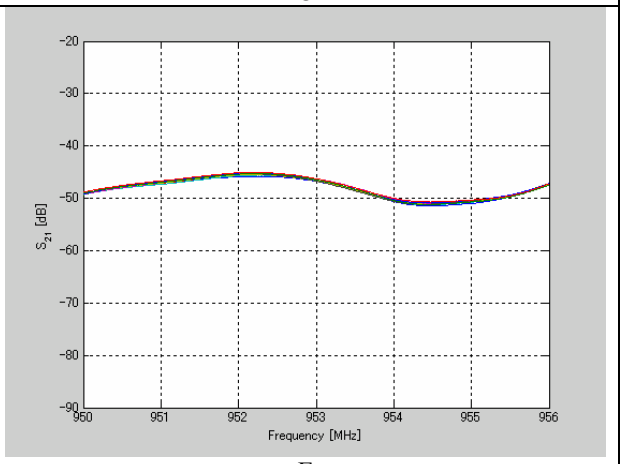
S21 [dB]
Frequency [MHz]

E

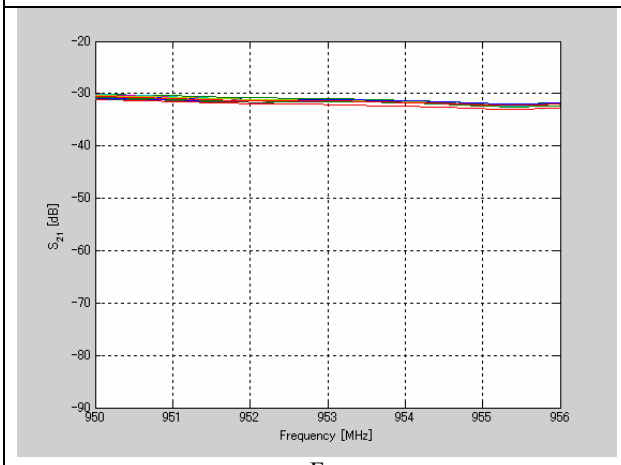
S21 [dB]
Frequency [MHz]

F

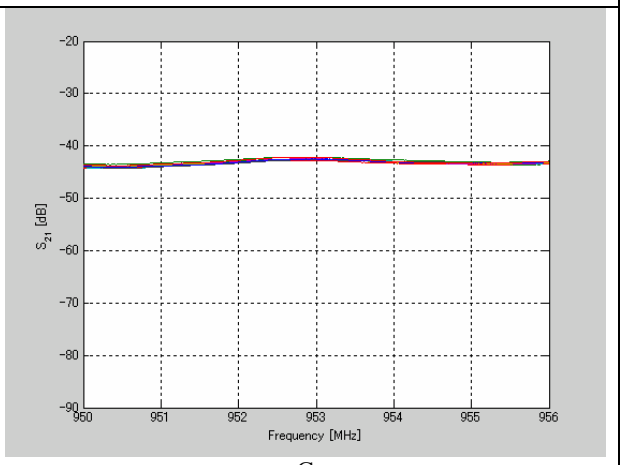
S21 [dB]
Frequency [MHz]

G

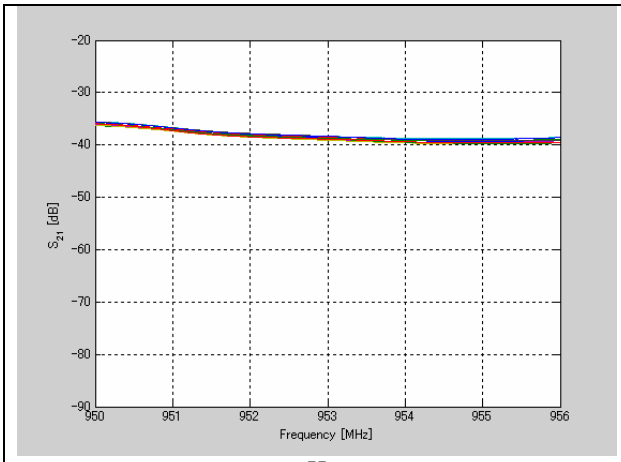

H

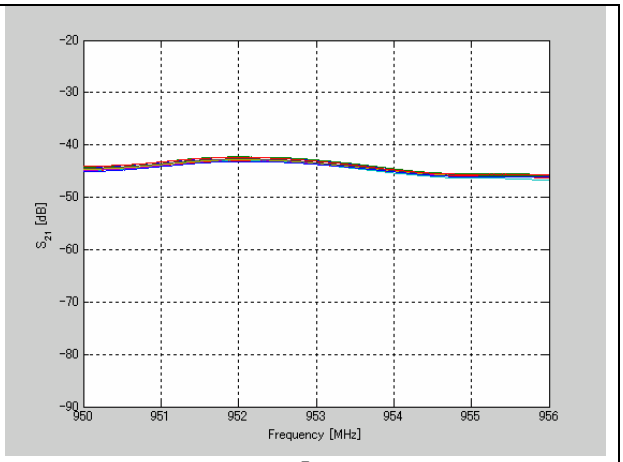

I

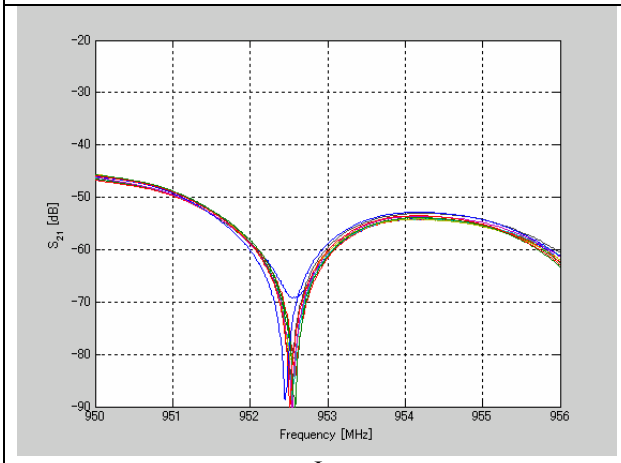

J

(d) 2.4GHz band (2.4 - 2.5 GHz)

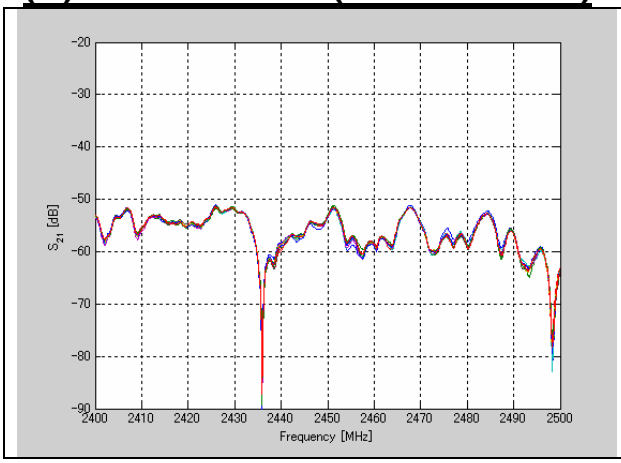

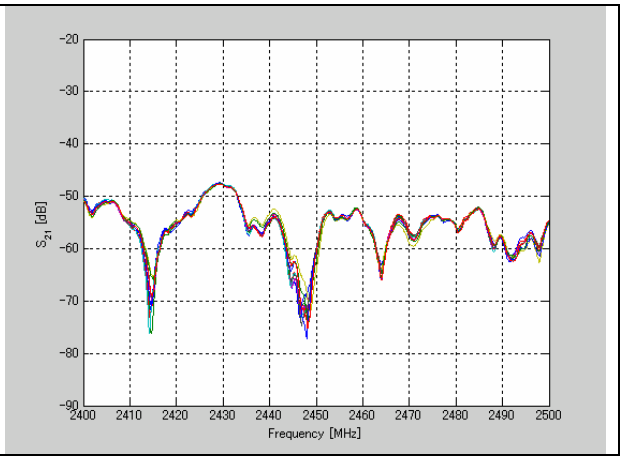

A-1	A-2
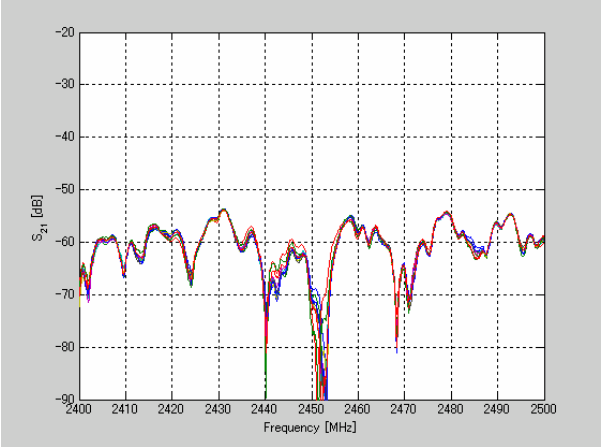	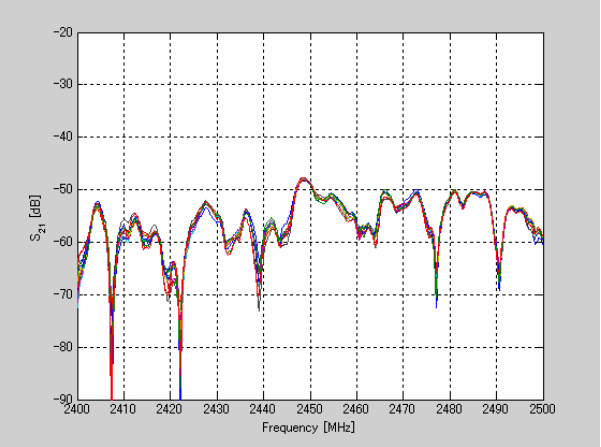
B	C
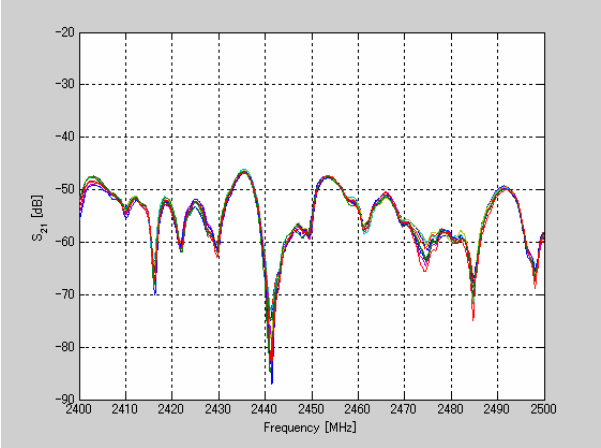	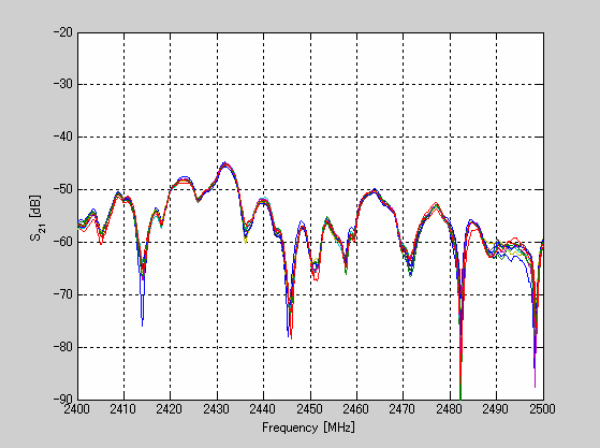
D	E
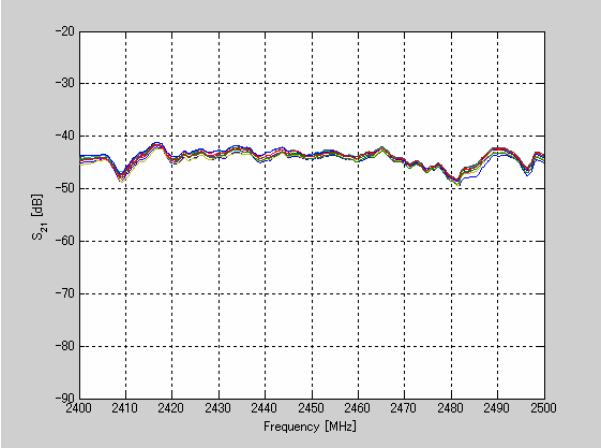	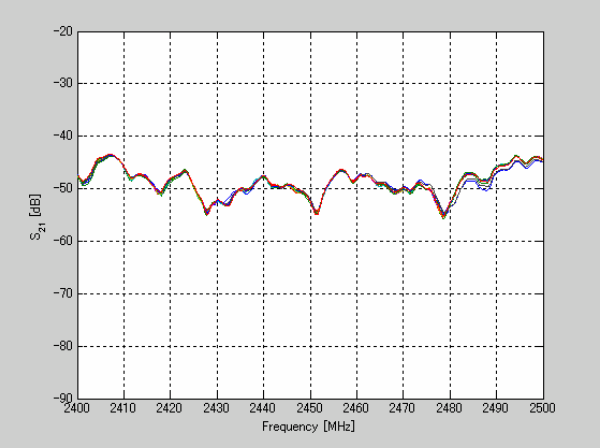
F	G

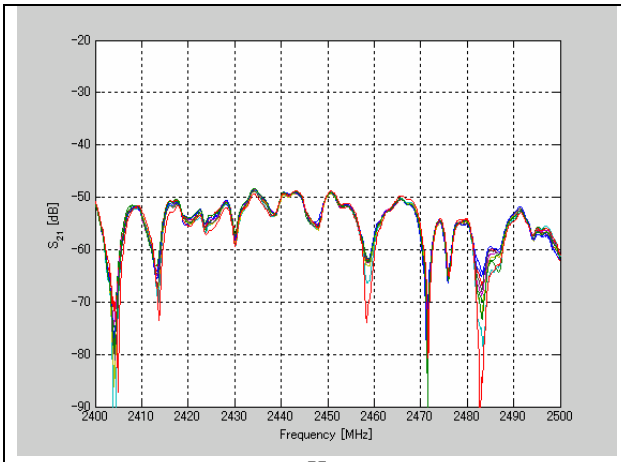

H

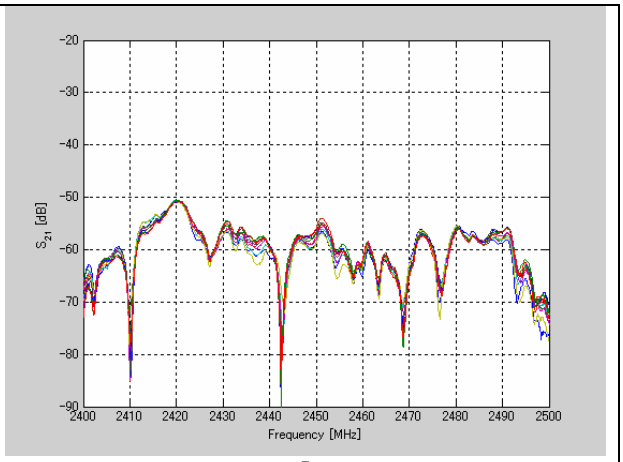

I

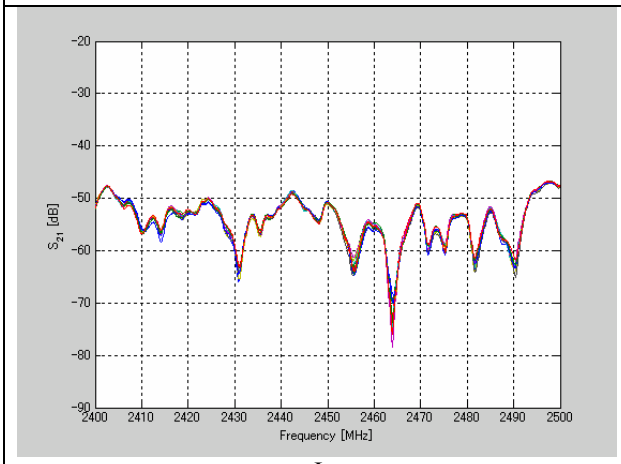

J

(e) UWB band (3 - 11GHz)

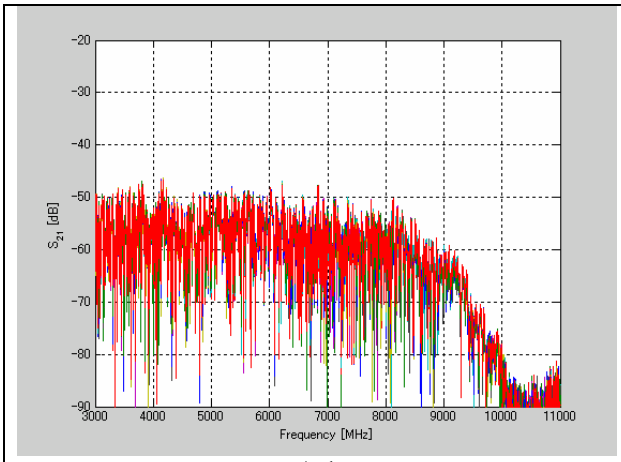
S21 [dB]
Frequency [MHz]

A-1

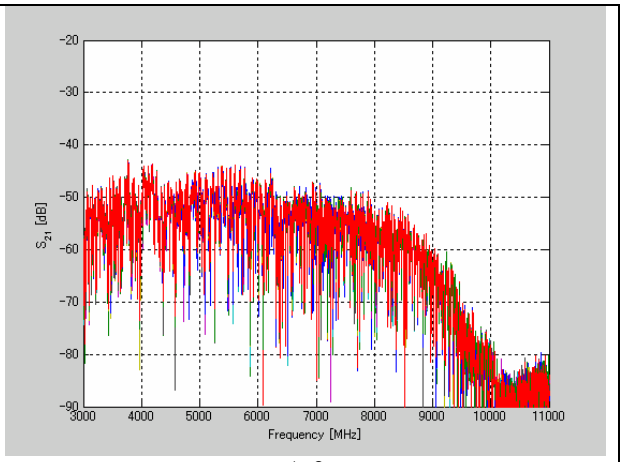
S21 [dB]
Frequency [MHz]

A-2

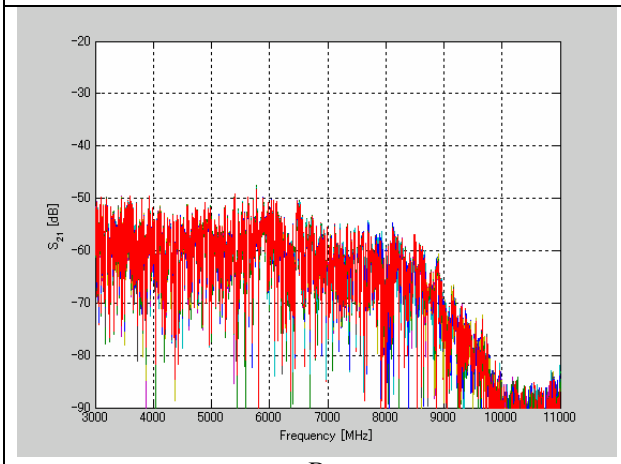
S21 [dB]
Frequency [MHz]

B

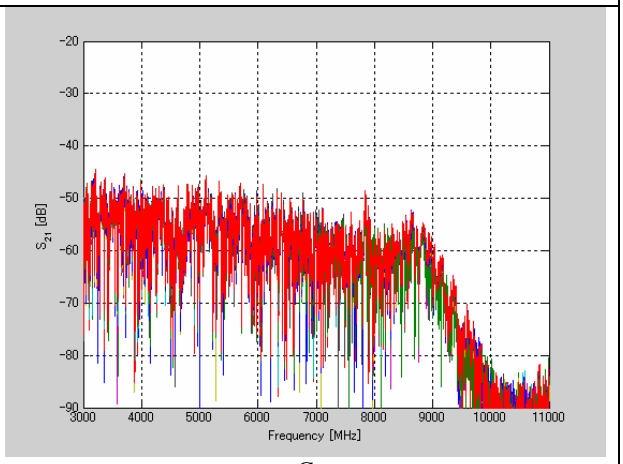
S21 [dB]
Frequency [MHz]

C

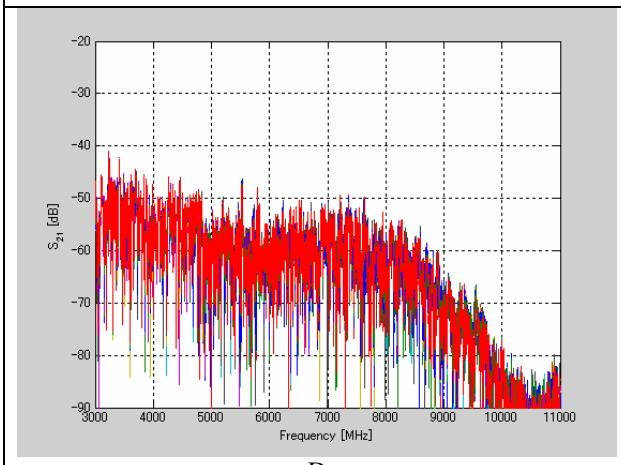
S21 [dB]
Frequency [MHz]

D

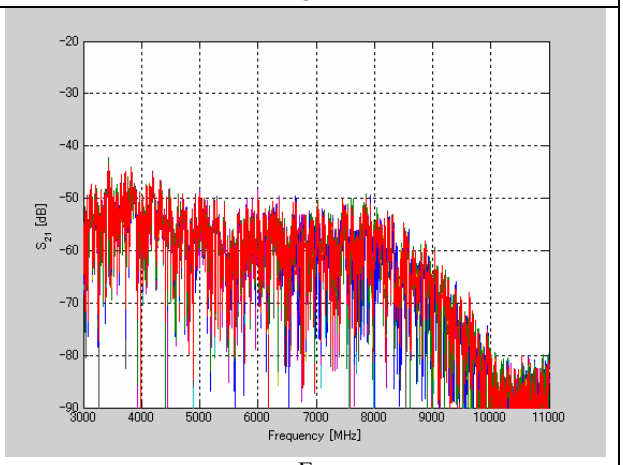
S21 [dB]
Frequency [MHz]

E

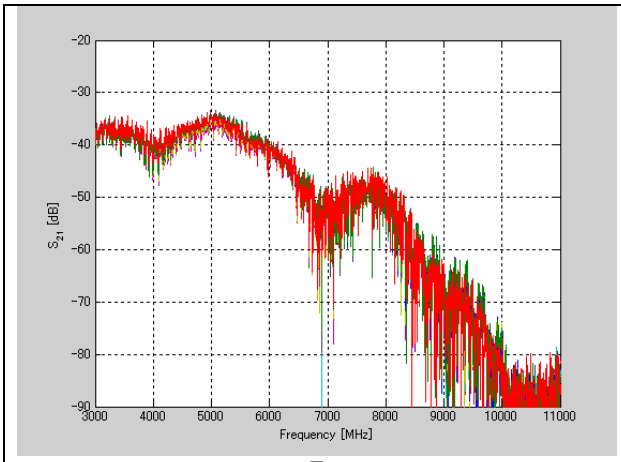
-20
-30
-40
-50
-60
-70
-80
-90
S_{21} [dB]
3000 4000 5000 6000 7000 8000 9000 10000 11000
Frequency [MHz]

F

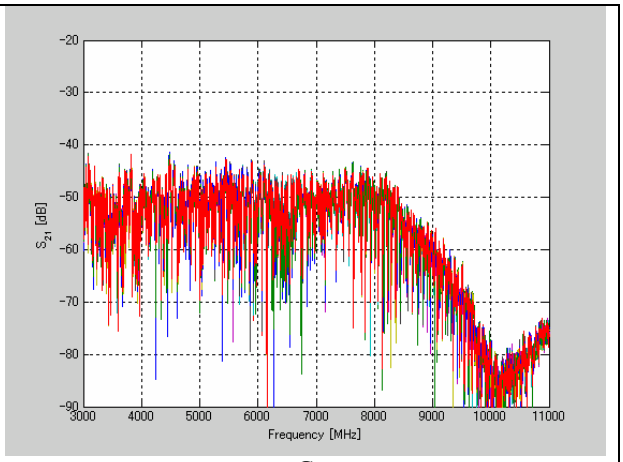
-20
-30
-40
-50
-60
-70
-80
-90
S_{21} [dB]
3000 4000 5000 6000 7000 8000 9000 10000 11000
Frequency [MHz]

G

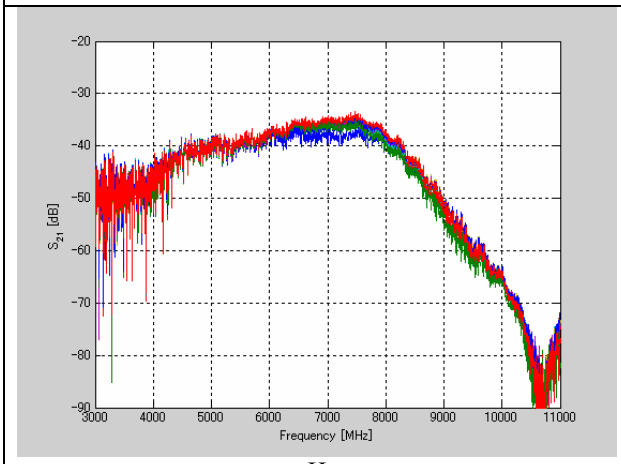
-20
-30
-40
-50
-60
-70
-80
-90
S_{21} [dB]
3000 4000 5000 6000 7000 8000 9000 10000 11000
Frequency [MHz]

H

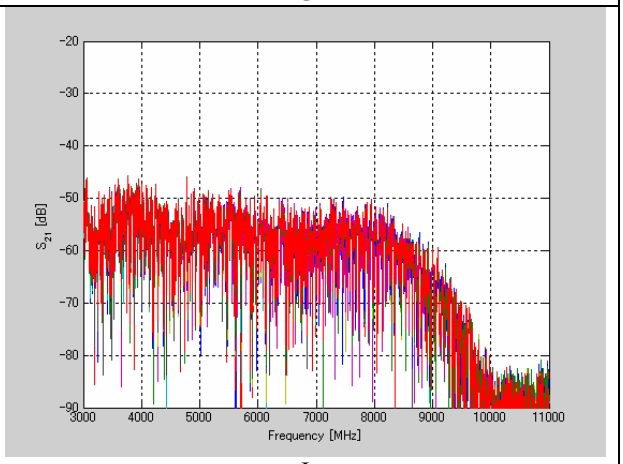
-20
-30
-40
-50
-60
-70
-80
-90
S_{21} [dB]
3000 4000 5000 6000 7000 8000 9000 10000 11000
Frequency [MHz]

I

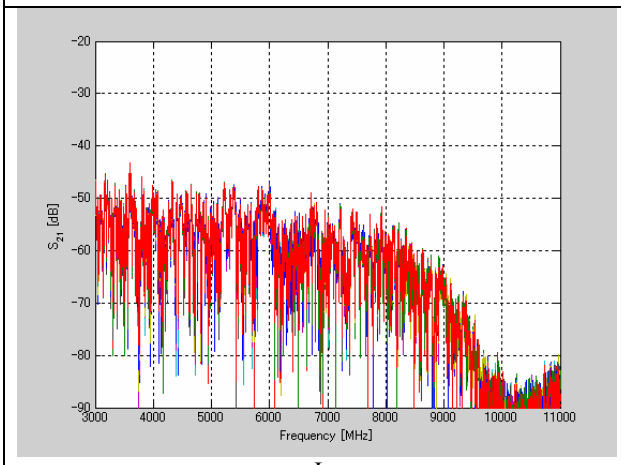
-20
-30
-40
-50
-60
-70
-80
-90
S_{21} [dB]
3000 4000 5000 6000 7000 8000 9000 10000 11000
Frequency [MHz]

J

A. 2 Measurement results in an anechoic chamber
(a) 400MHz band (400 - 450 MHz)

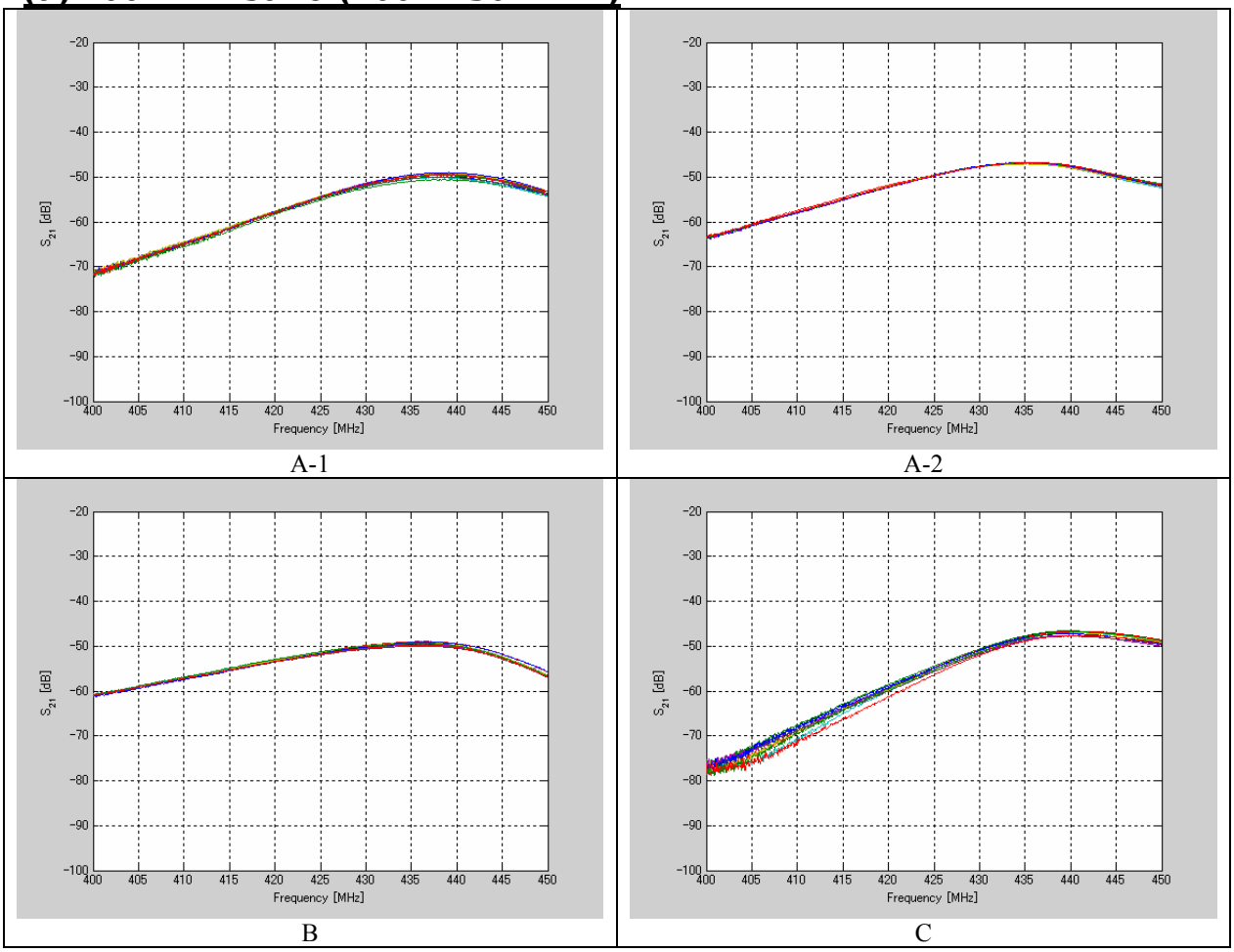

A-1 A-2

B C

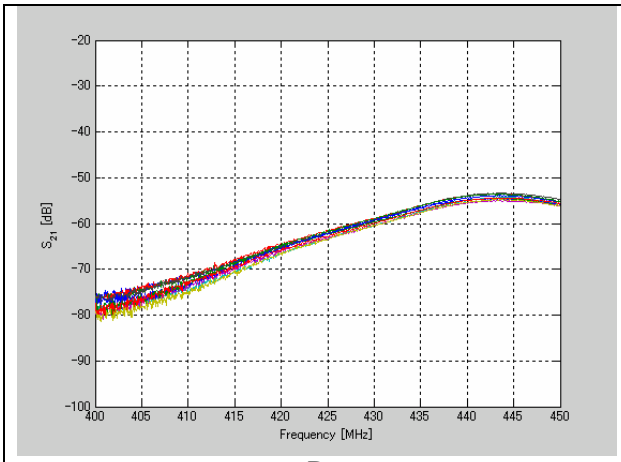
S21 [dB]
Frequency [MHz]

D

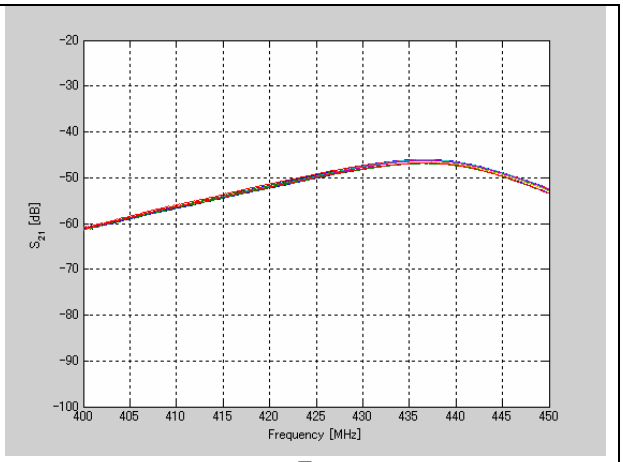
S21 [dB]
Frequency [MHz]

E

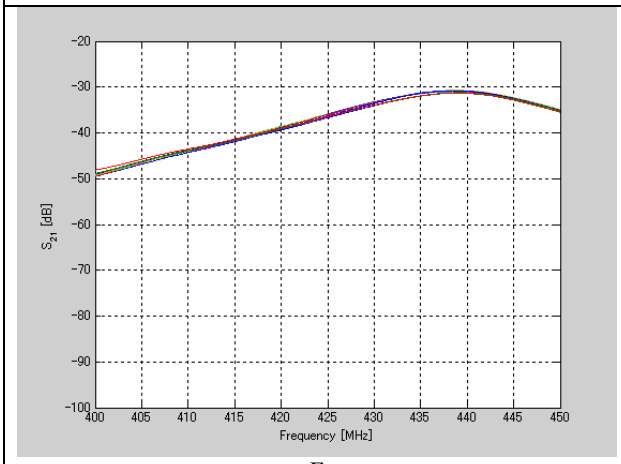
S21 [dB]
Frequency [MHz]

F

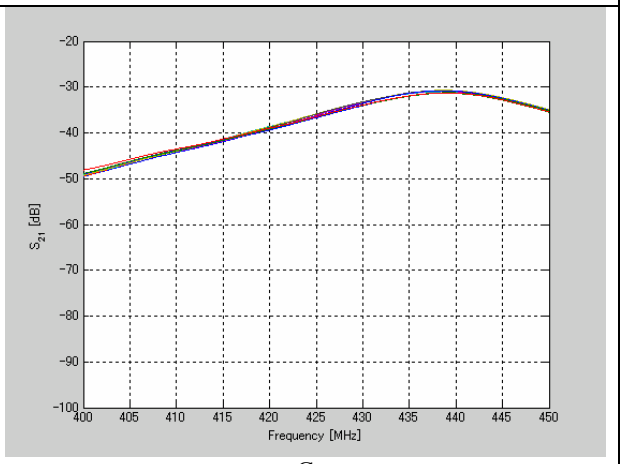
S21 [dB]
Frequency [MHz]

G

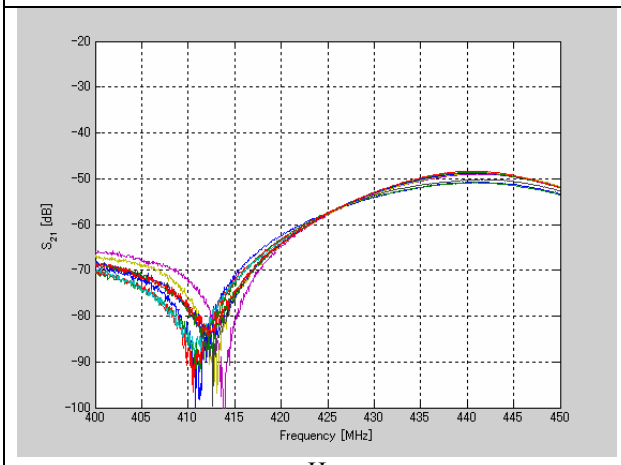
S21 [dB]
Frequency [MHz]

H

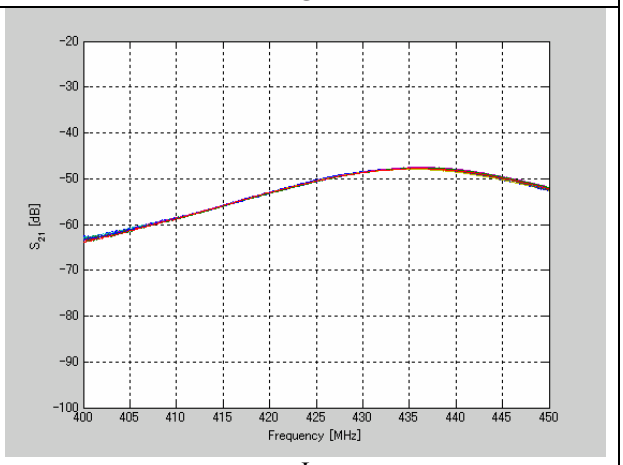
S21 [dB]
Frequency [MHz]

I

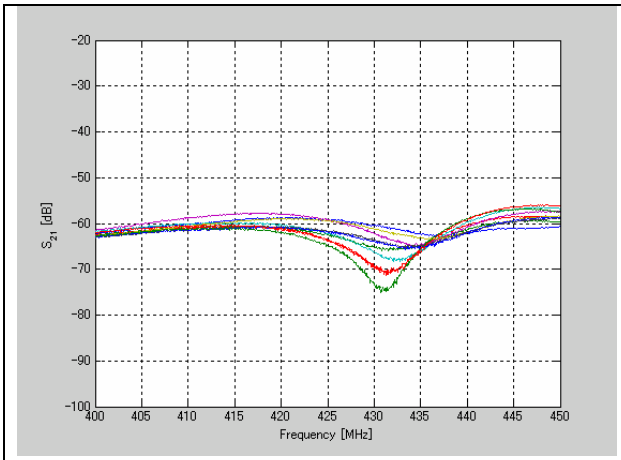

J

(b) 600MHz band (608 – 614 MHz)

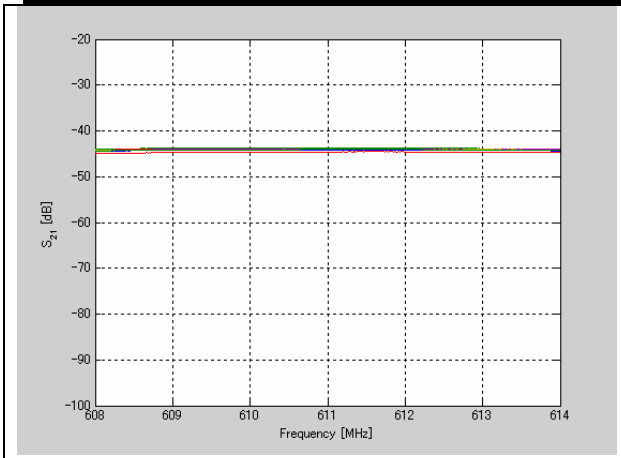

A-1

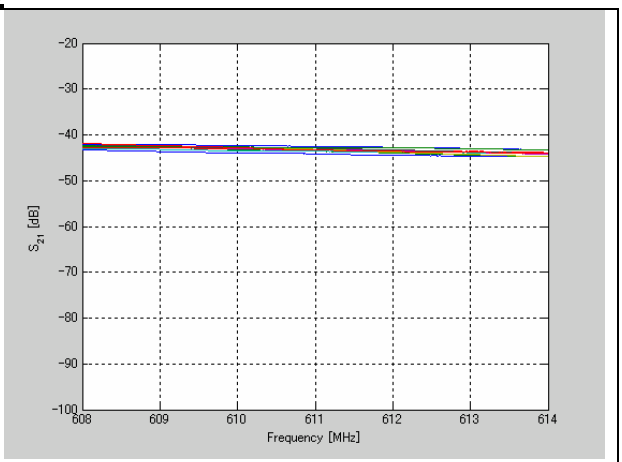

A-2

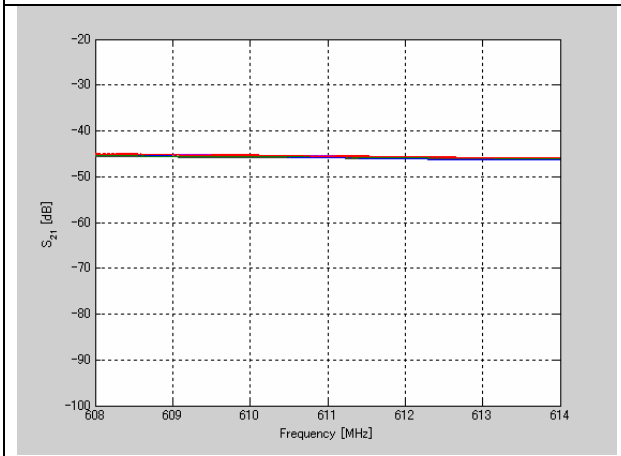

B

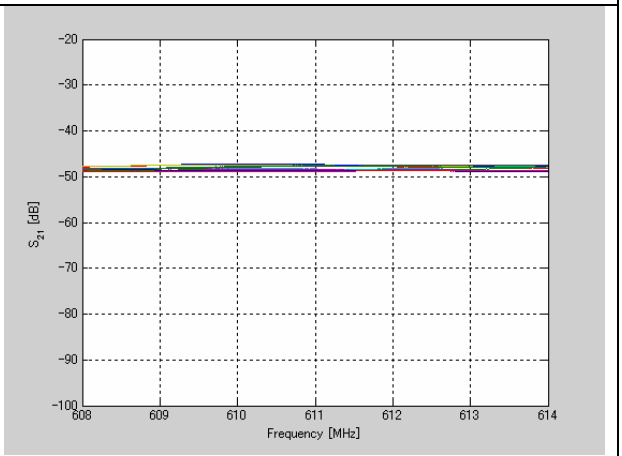

C

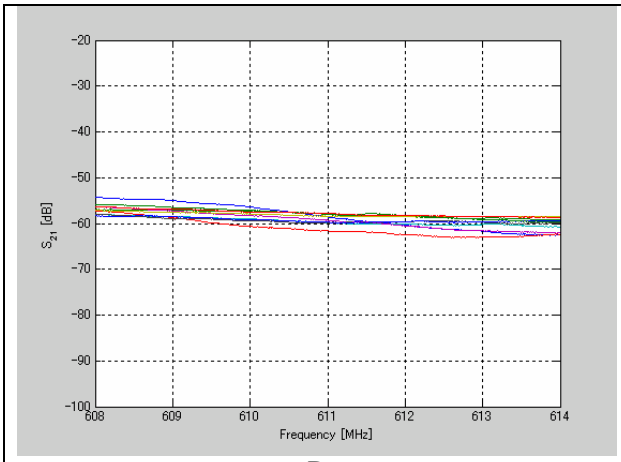
S21 [dB]
Frequency [MHz]

D

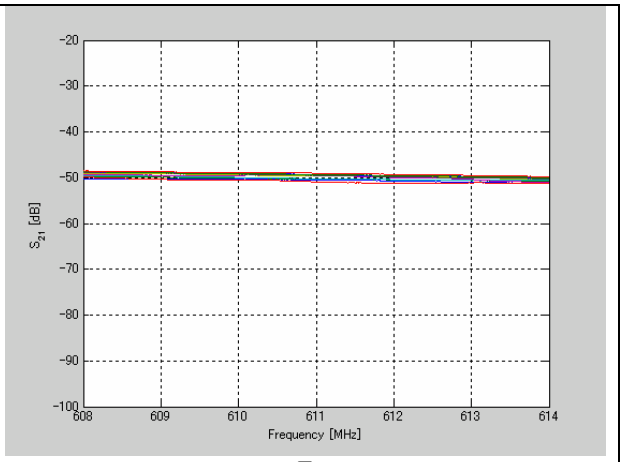
S21 [dB]
Frequency [MHz]

E

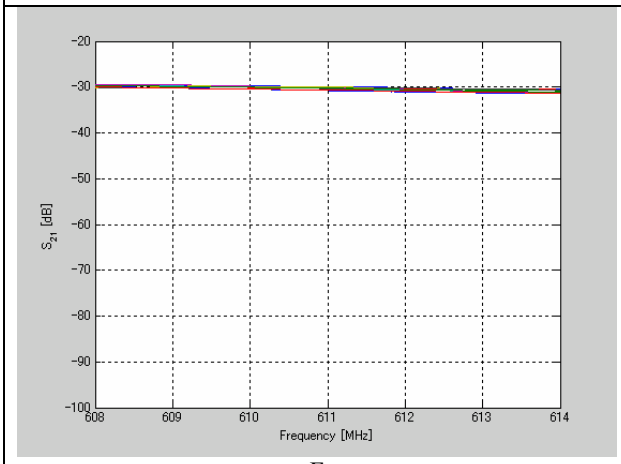
S21 [dB]
Frequency [MHz]

F

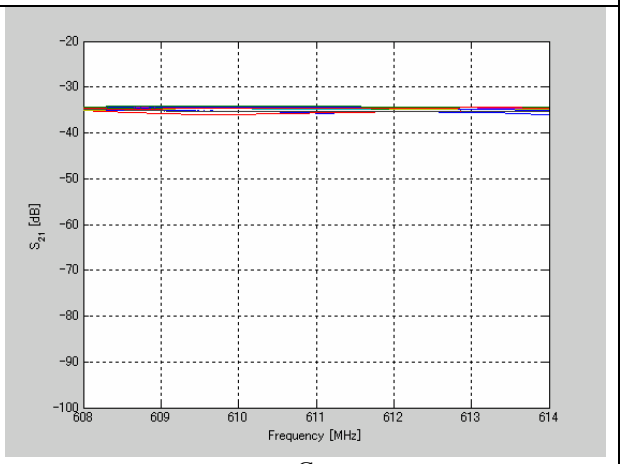
S21 [dB]
Frequency [MHz]

G

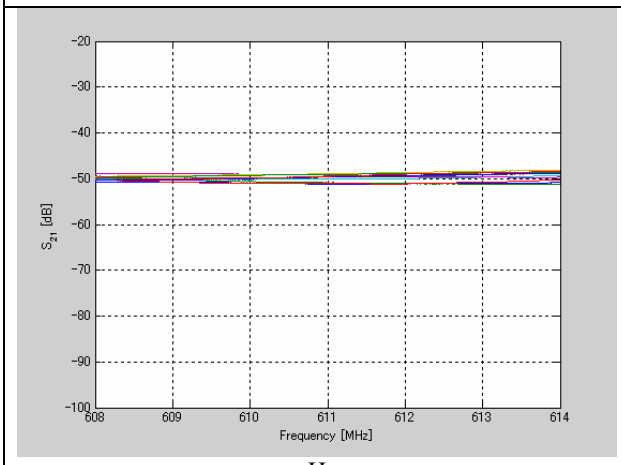
S21 [dB]
Frequency [MHz]

H

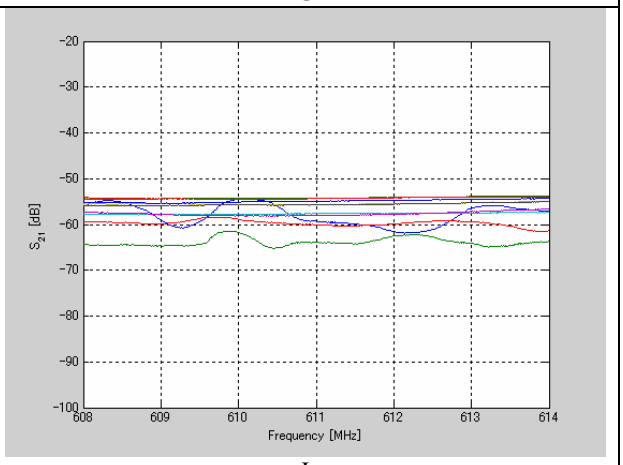
S21 [dB]
Frequency [MHz]

I

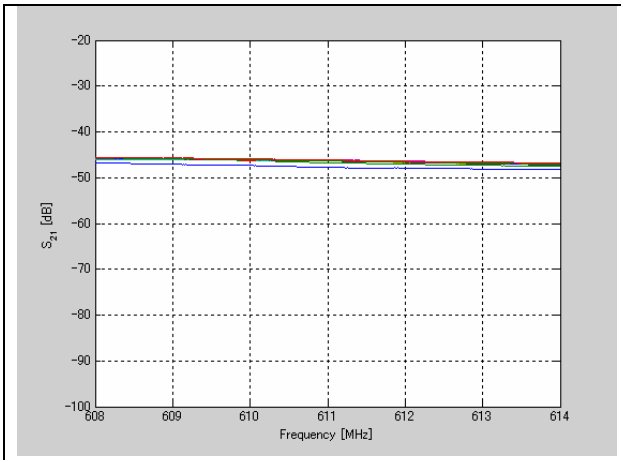

J

(c)900MHz band (950 - 956 MHz)

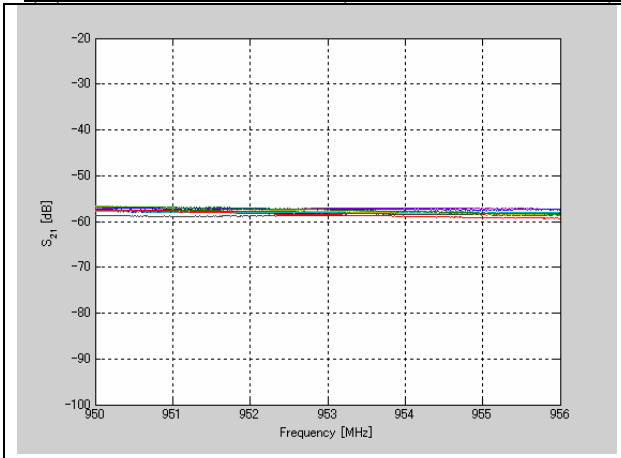

A-1

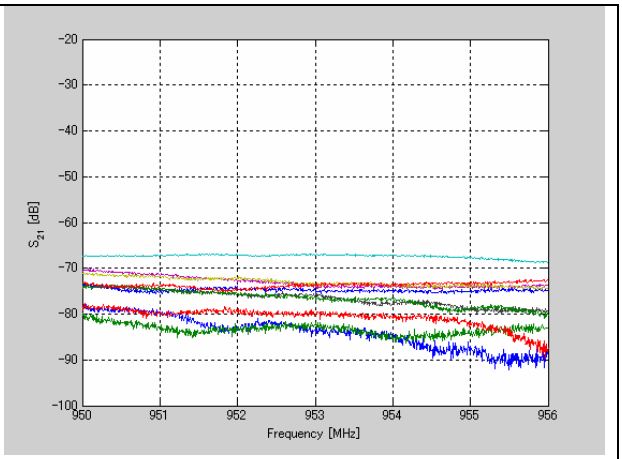

A-2

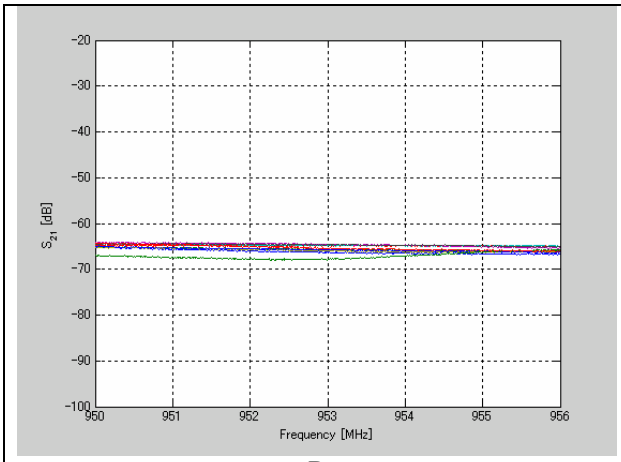
-20
-30
-40
-50
-60
-70
-80
-90
-100
S21 [dB]
950
951
952
953
954
955
956
Frequency [MHz]

B

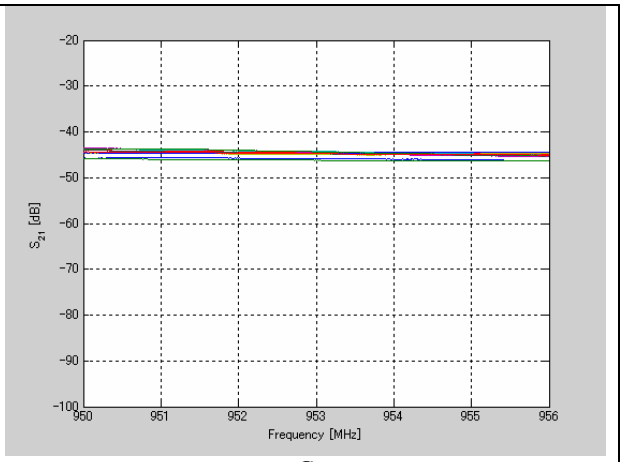
-20
-30
-40
-50
-60
-70
-80
-90
-100
S21 [dB]
950
951
952
953
954
955
956
Frequency [MHz]

C

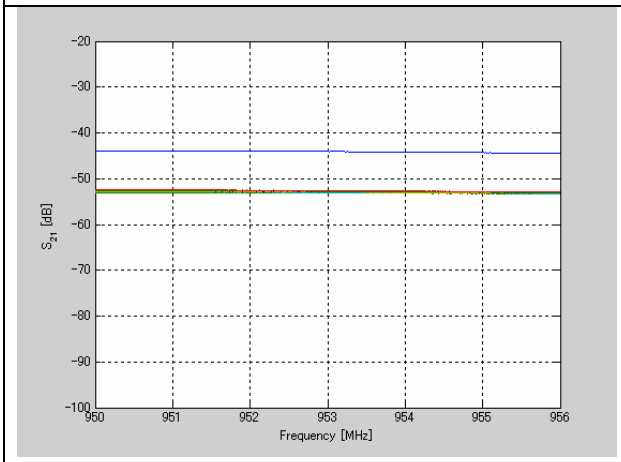
-20
-30
-40
-50
-60
-70
-80
-90
-100
S21 [dB]
950
951
952
953
954
955
956
Frequency [MHz]

D

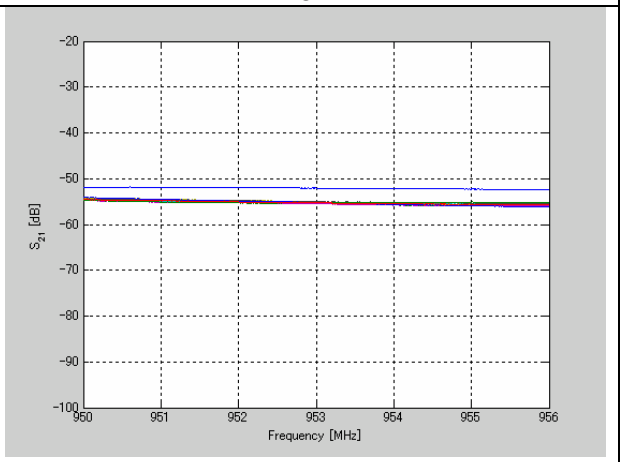
-20
-30
-40
-50
-60
-70
-80
-90
-100
S21 [dB]
950
951
952
953
954
955
956
Frequency [MHz]

E

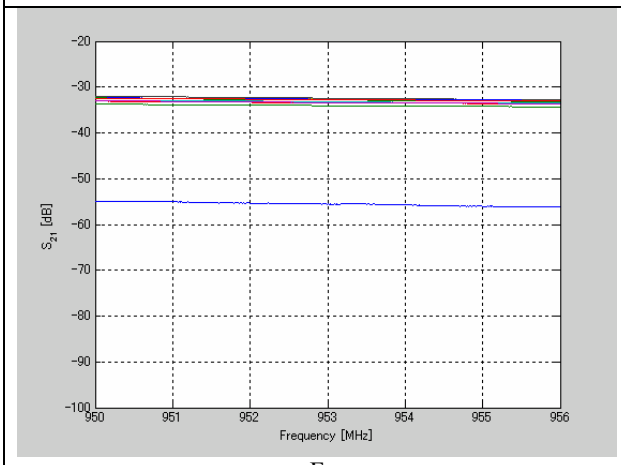
-20
-30
-40
-50
-60
-70
-80
-90
-100
S21 [dB]
950
951
952
953
954
955
956
Frequency [MHz]

F

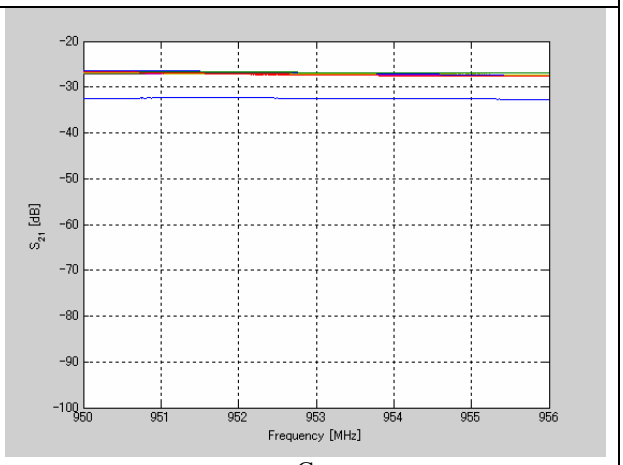
-20
-30
-40
-50
-60
-70
-80
-90
-100
S21 [dB]
950
951
952
953
954
955
956
Frequency [MHz]

G

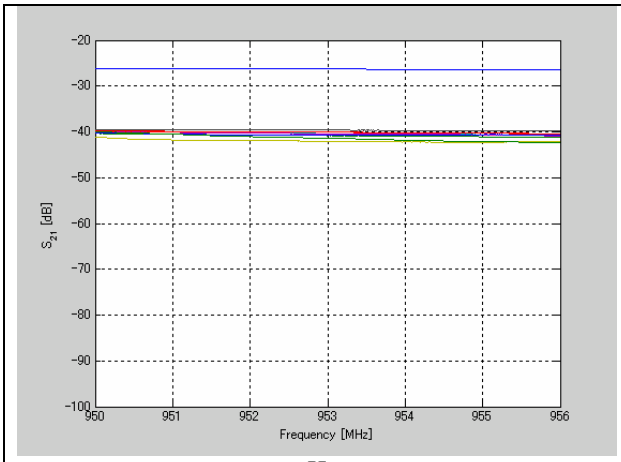

H

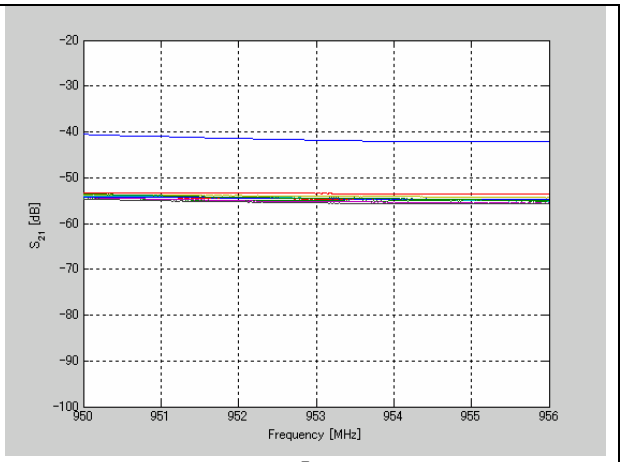

I

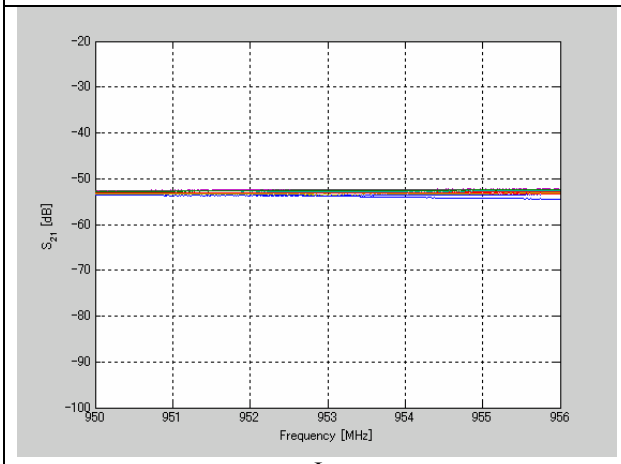

J

(d) 2.4GHz band (2.4 - 2.5 GHz)

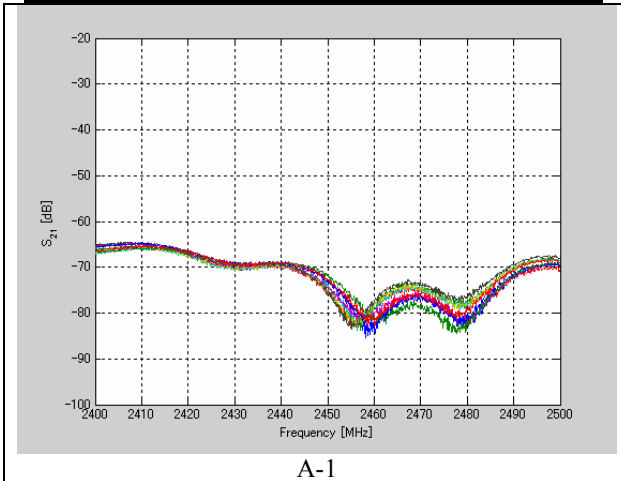

A-1

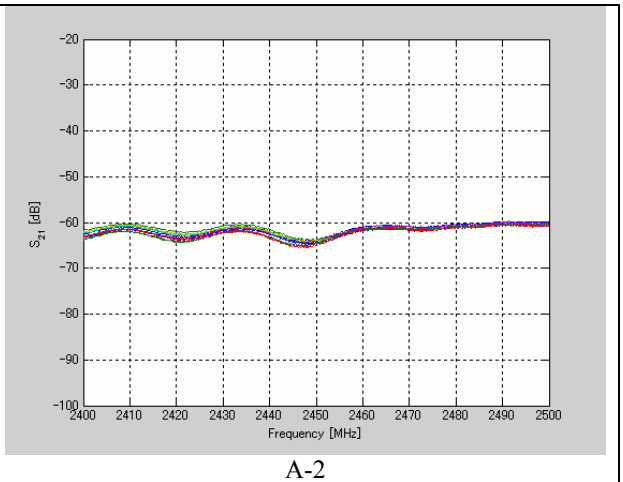

A-2

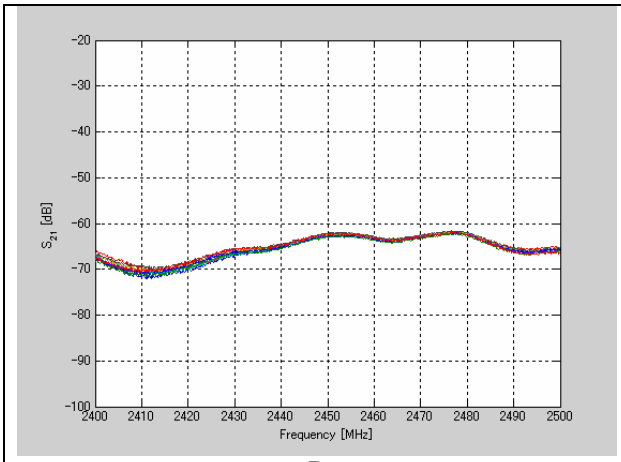
S21 [dB]
Frequency [MHz]

B

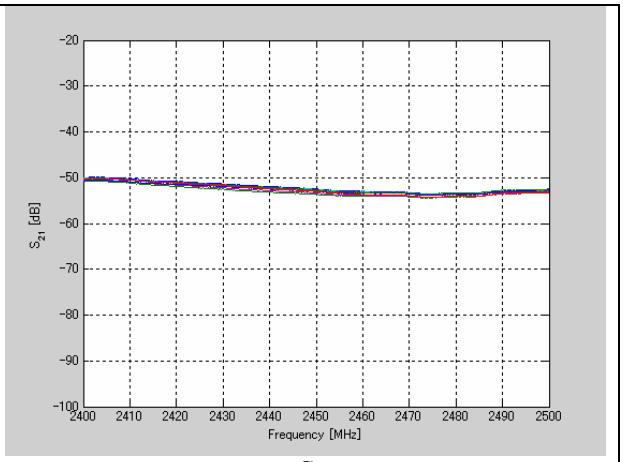
S21 [dB]
Frequency [MHz]

C

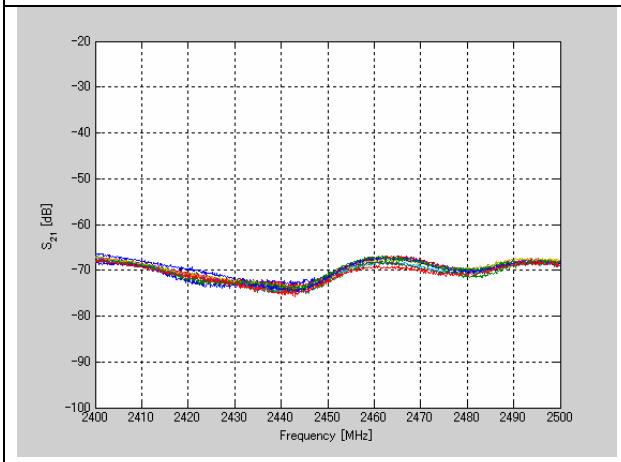
S21 [dB]
Frequency [MHz]

D

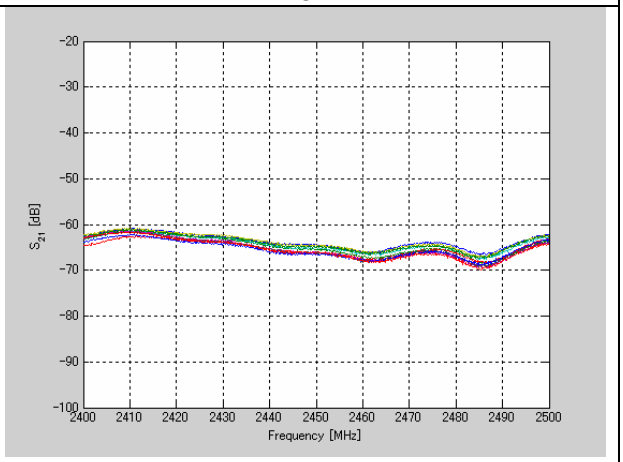
S21 [dB]
Frequency [MHz]

E

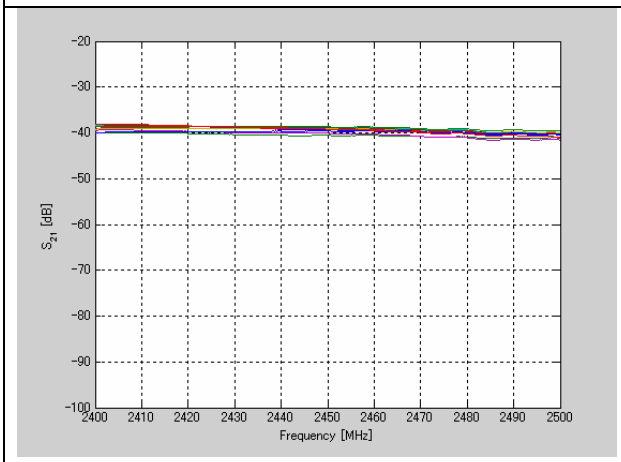
S21 [dB]
Frequency [MHz]

F

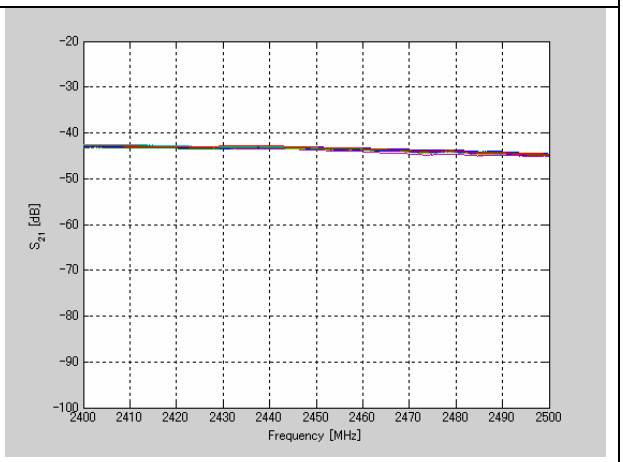
S21 [dB]
Frequency [MHz]

G

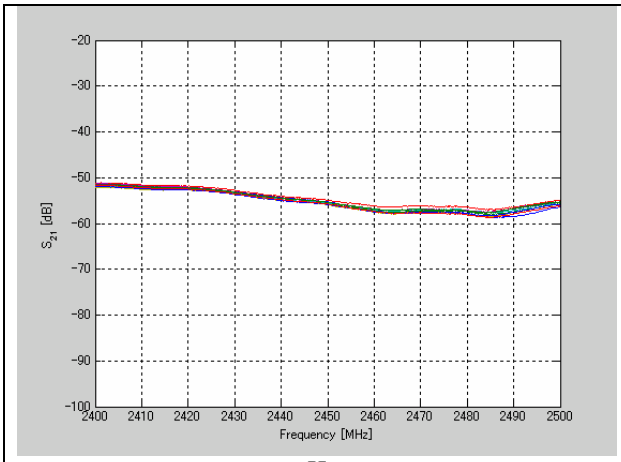

H

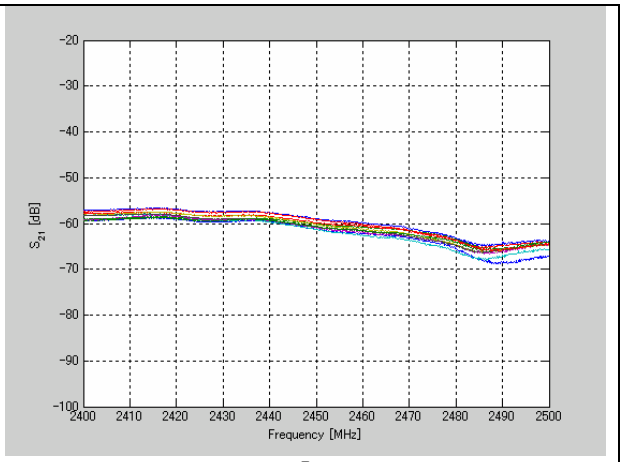

I

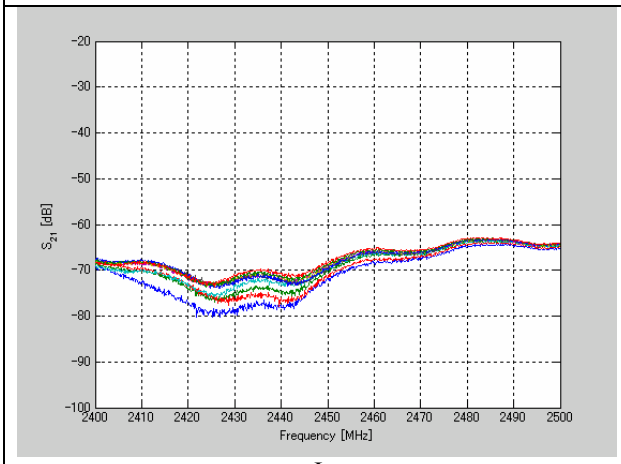

J

(e) UWB band (3 - 11 GHz)

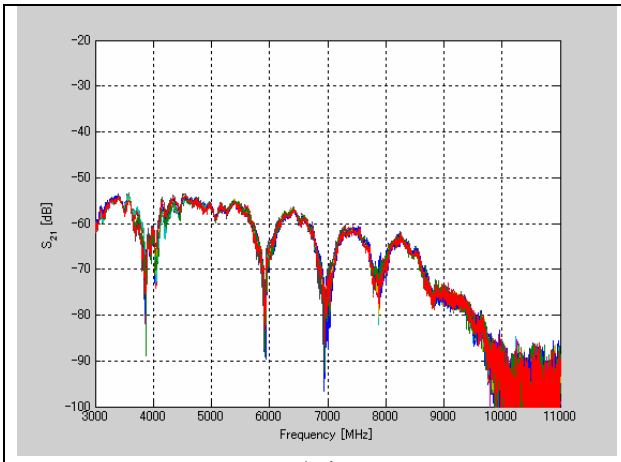
S21 [dB]
Frequency [MHz]

A-1

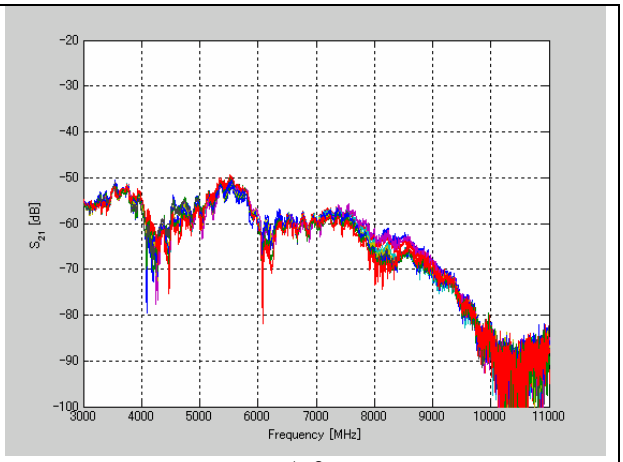
S21 [dB]
Frequency [MHz]

A-2

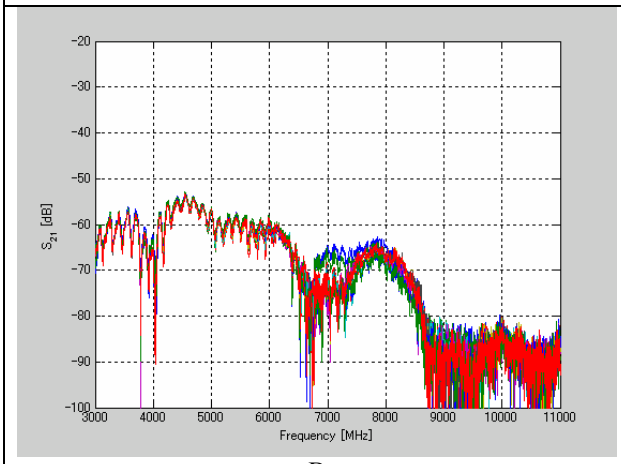
S21 [dB]
Frequency [MHz]

B

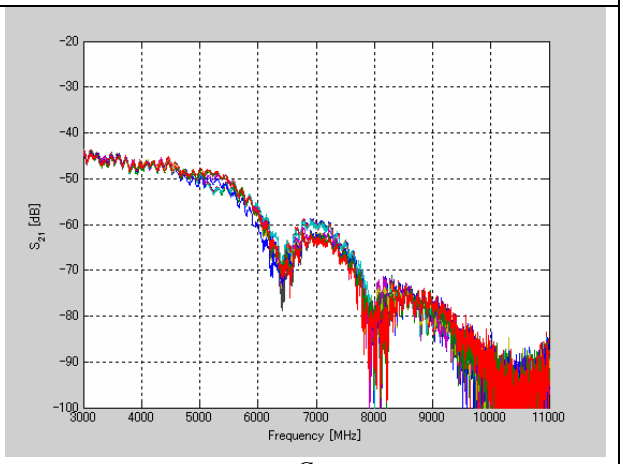
S21 [dB]
Frequency [MHz]

C

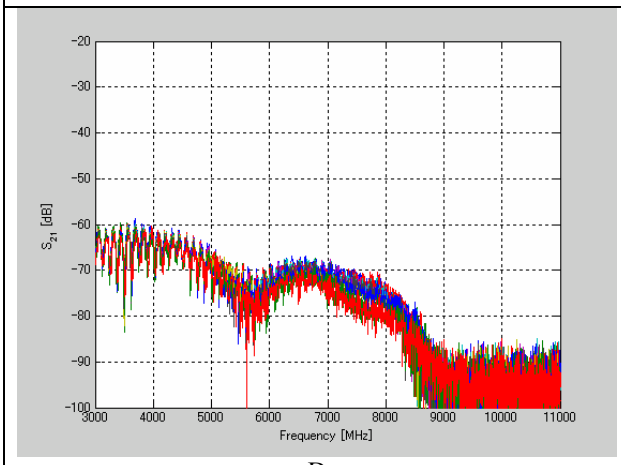
S21 [dB]
Frequency [MHz]

D

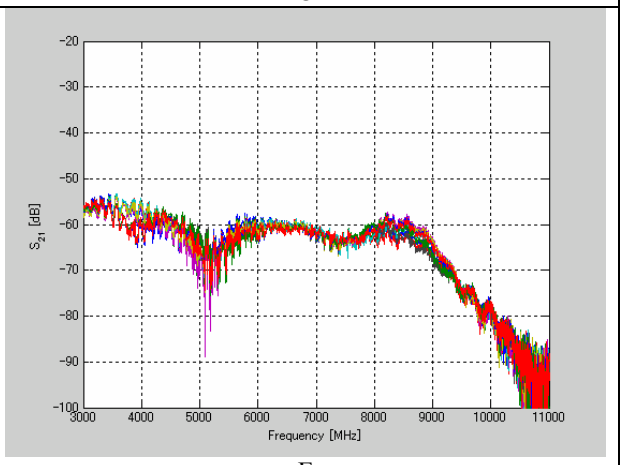
S21 [dB]
Frequency [MHz]

E

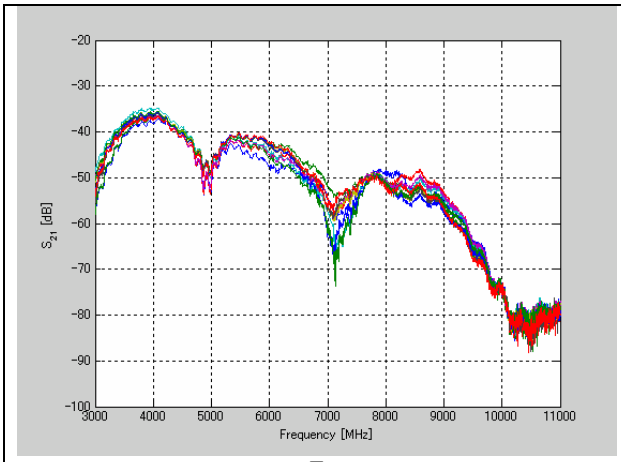
S21 [dB]
Frequency [MHz]

F

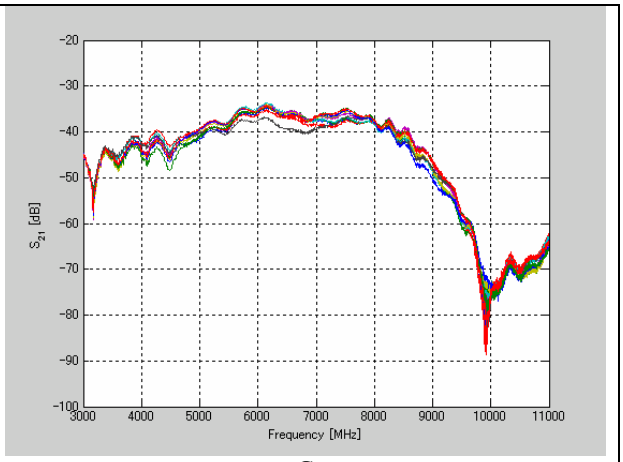
S21 [dB]
Frequency [MHz]

G

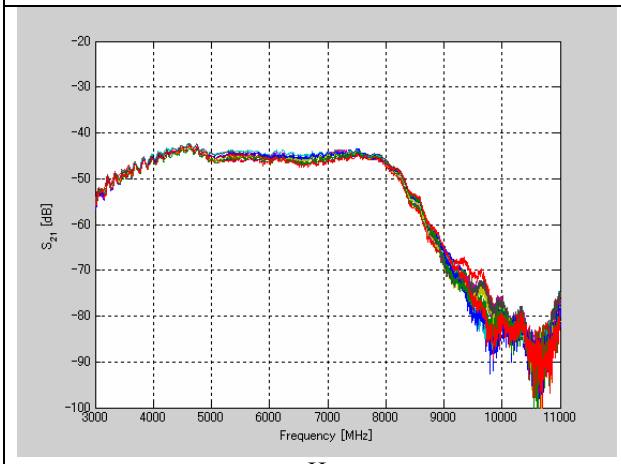
S21 [dB]
Frequency [MHz]

H

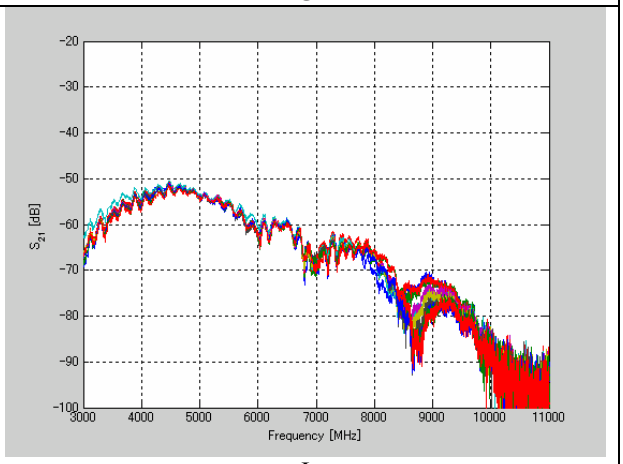
S21 [dB]
Frequency [MHz]

I

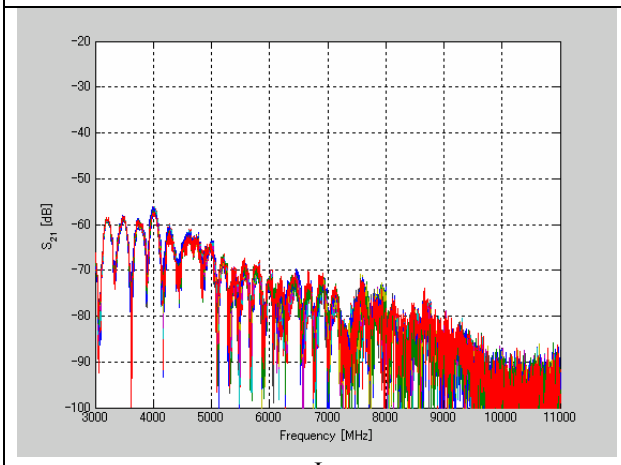
S21 [dB]
Frequency [MHz]

J

Appendix B. Examples of MATLAB codes for the channel models

1. CM3

1.1 Path loss

```
N_ch     = 100;          % # of path loss realizations
distance = 1000;         % unit: mm (the distance should be more than 100 mm.)

if distance <= 100
   fprintf('! WARNING ! The distance is less than 100 mm.')
end

% ==================== Channel parameter ===============
frequency   = 1;  % 1: 400MHz, 2: 600MHz, 3: 900MHz, 4: 2450MHz, 5: UWB
if frequency == 1
   a   = 3.00;
   b   = 34.6;
   sigma_s = 4.63;
elseif frequency == 2
   a   = 16.7;
   b   = -0.45;
   sigma_s = 5.99;
elseif frequency == 3
   a   = 15.5;
   b   = 5.38;
   sigma_s = 5.35;
elseif frequency == 4
   a   = 6.60;
   b   = 36.1;
   sigma_s = 3.80;
elseif frequency == 5
   a   = 19.2;
   b   = 3.38;
   sigma_s = 4.40;
end
% ======================================================
% =============== Path loss realizations ===============
% -- Path loss in dB
PL     = a*log10(distance)+b+sigma_s*randn(1,N_ch);
% ======================================================
```

1.2 Power delay profile

```
N_ch    = 100;  % # of realization on channel impulse response (CIR)

% ================== Parameters ==================
L_av       = 20.2;         % Average number of the arrival paths
sigma_s    = 5.94;         % Standard deviation on the amplitude level
Gamma      = 61.3;         % Exponential decay factor
gamma_0    = -3.3;         % Rice factor
lambda     = 6.18;         % Time difference between neighboring arrival paths
ts         = 5.0125*10^-10; % Sampling time
% ============= Calculate CIR realizations =============
for n_ch = 1 :N_ch
   T_p    = 0;
   N_path = max(1,poissrnd(L_av));
   for n_p = 1 :N_path
      if T_p == 0
         amp_path = 1;
      else
         amp_path = 10^((10*log10(exp(-T_p/Gamma))+gamma_0+sigma_s*randn)/20);
      end
      t(n_ch,n_p) = T_p;
      h(n_ch,n_p) = amp_path*rand(1)*2*pi;
      T_p = T_p + poissrnd(lambda)*ts;
   end
   h_norm(n_ch,1:N_path) = h(n_ch,1:N_path)/sqrt(sum(abs(h(n_ch,:))));
end
```

2. CM4

```
N_ch    = 100;

% ================== Parameters ==================
L          = 200;          % # of arrival paths
body_direction = 1;        % 1: 0 deg, 2: 90 deg, 3: 180 deg, 4: 270 deg
ts         = 5.0125*10^-10; % Sampling time
% ---
if body_direction == 1
   Gamma      = 0.224;        % [ns]
   delta_k    = 6.4;          % [dB]
```

```
   sigma      = 7.30;         % [dB]
elseif body_direction == 2
   Gamma      = 0.184;        % [ns]
   delta_k    = 3.0;          % [dB]
   sigma      = 7.08;         % [dB]
elseif body_direction == 3
   Gamma      = 0.187;        % [ns]
   delta_k    = 0;            % [dB]
   sigma      = 7.03;         % [dB]
elseif body_direction == 4
   Gamma      = 0.191;        % [ns]
   delta_k    = 1.5;          % [dB]
   sigma      = 7.19;         % [dB]
end
% ================================================
% ================= Realizations ==================
for n_ch = 1 :N_ch
   T_p    = 0;
   for n_p = 1 :L
      if T_p == 0
         amp_path = 1;
      else
         amp_path = exp(-T_p*10^9/Gamma-delta_k*log(10)/10);
      end
      t(n_ch,n_p) = T_p;
      h(n_ch,n_p) = amp_path*rand(1)*2*pi;
      T_p = T_p + ts;
   end
   h_norm(n_ch,1:L) = h(n_ch,1:L)/sqrt(sum(abs(h(n_ch,1:L)).^2));
end
% ================================================
```

3. CM2

```
N_ch     = 100;          % # of path loss realizations
distance = 10;           % unit: cm
theta    = 0;            % Antenna angle between implanted and outside antennas [rad]

% ================== Channel parameter ===============
a        = 1.92;
b        = 39.85;
```

```
sigma_N  = 6.59;
x_c      = 0.145;
% ================================================
% ============== Path loss realizations ==========
% -- Path loss in dB
P_theta  = 20*log10(cos(theta)*(1-x_c)+x_c);
PL       = a*distance+b+P_theta+sigma_N*randn(1,N_ch);
% ================================================
```